Advanced Concepts in Photovoltaics

Edited by

Arthur J Nozik
National Renewable Energy Laboratory, Colorado, USA
Email: anozik@nrel.gov

Gavin Conibeer
University of New South Wales, Sydney, Australia
Email: g.conibeer@unsw.edu.au

Matthew C Beard
National Renewable Energy Laboratory, Colorado, USA
Email: matt.beard@nrel.gov

RSC Energy and Environment Series No. 11

ISBN: 978-1-84973-591-9
PDF eISBN: 978-1-84973-995-5
ISSN: 2044-0774

A catalogue record for this book is available from the British Library

Published by The Royal Society of Chemistry,
Thomas Graham House, Science Park, Milton Road,
Cambridge CB4 0WF, UK

Registered Charity Number 207890

For further information see our web site at www.rsc.org

CHAPTER 16

Quantum Rectennas for Photovoltaics

FENG YU,[a] GARRET MODDEL[b] AND RICHARD CORKISH*[a]

[a] School of Photovoltaic and Renewable Energy Engineering and Australia-US Institute for Advanced Photovoltaics, The University of New South Wales, Sydney 2052, Australia; [b] Department of Electrical, Computer, and Energy Engineering, University of Colorado, Boulder CO 80309-0425, USA
*Email: r.corkish@unsw.edu.au

16.1 Introduction

Quantum antennas for photovoltaics are special cases in the rapidly growing field of optical antennas. An optical antenna is 'a device that converts freely propagating optical radiation into localized energy, and *vice versa*'.[1–4] Quantum antennas for photovoltaics are specifically required to couple optical solar radiation to a load, commonly via a rectifier.[5] The combined antenna and rectifier is termed a 'rectenna'.

A rectenna, or rectifying antenna (Figure 16.1) is a device for the conversion of electromagnetic energy propagating through space to direct current electricity in a circuit, available to be delivered to a load or to storage. It has one or more elements, each consisting of an antenna, filter circuits and a rectifying diode or bridge rectifier either for each antenna element or for the power from several elements combined. They are under consideration as alternatives to conventional solar cells.

Conventional solar cells, with the exception of their reflection coatings, are quantum devices, only able to be understood through quantum physics. On the

RSC Energy and Environment Series No. 11
Advanced Concepts in Photovoltaics
Edited by Arthur J Nozik, Gavin Conibeer and Matthew C Beard

Published by the Royal Society of Chemistry, www.rsc.org

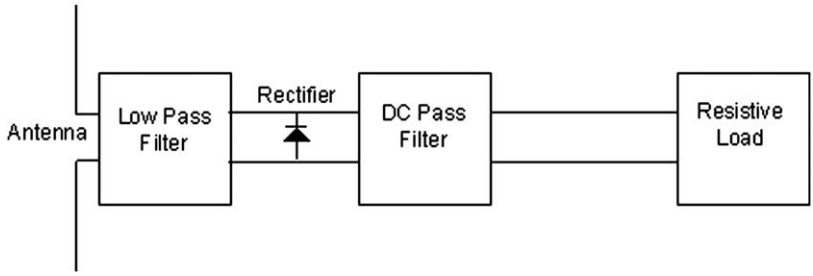

Figure 16.1 Conceptual structure of a rectenna. Reproduced from Corkish *et al.*[6]

other hand, the wave nature of light is routinely exploited at longer wavelengths in radio and microwave frequency bands for communications, heating and sensing. Photon energies are small at radio frequencies and a large number is required to produce significant power density. Engineers routinely use wave models for radiation in that regime. At shorter wavelengths, fewer photons are required for the same power density and particle models are commonly applied. In principle, there should be no reason why the electromagnetic wave technologies which are so successfully used for radio communications cannot be scaled to optical frequencies, although quantum models may be necessary for at least some aspects. However, there are significant practical issues, especially concerning the sub-millimeter size scales involved.

In parallel, antenna structures used to generate surface plasmons are exciting great interest in the physics and engineering communities, including in the photovoltaics arena.[7,8] In these applications, including the enhancement of light absorption by dye molecules,[9] nanoscale metallic particles absorb and re-emit light and are used to intensify light absorption in conventional solar cells, even beyond the ergodic limit. These applications are beyond the scope of this article and are considered elsewhere.[10,11]

There are significant overlaps and common interests with radioastronomy. A solar rectenna is similar to a simple radiotelescope or radiometer[12] but differs in that the radio telescope needs to measure the intensity of the radiative power received by the antenna, often with a square-law detector which produces an output voltage proportional to the input power, while the rectenna needs to convert that power to useful DC electricity. In terms of a solar cell analogy, the radiotelescope observes the open circuit voltage while the rectenna extracts power at the maximum power point.

16.2 History of Quantum Antennas for Photovoltaics Research

16.2.1 Optical and Infrared Rectennas

This field has been briefly reviewed in the past by Corkish *et al.*,[6,13] Goswami[14] and Rzykov *et al.*[15] and more recently and extensively by

Eliasson,[16] and Moddel and Grover.[17] The concept of using antennas to convert solar energy to rectified electricity first appeared in the literature in the early 1970s when Bailey,[18] Bailey *et al.*,[19] and Fletcher and Bailey[20] proposed the idea of collecting solar energy with devices based on the wave nature of light. He suggested artificial pyramid or cone structures like those in eyes. He describes pairs of the pyramids as modified dipole antennas, each pair electrically connected to a diode (half-wave rectifier), low-pass filter and load. The antenna elements needed to be several wavelengths long to permit easier fabrication (Figure 16.2).

Marks[21] patented the use of arrays of submicron crossed $\lambda/2$ dipoles on an insulating sheet with fast full-wave rectification (Figure 16.3). Marks' structure is essentially a conventional broadside array antenna with the output signal from several dipoles feeding into a transmission line to convey their combined power to a rectifier. This design requires the oscillations from each dipole to add in phase. Marks also patented devices to collect and convert solar energy using solidified sheets containing oriented metal dipole particles or molecules[22] and his later patent[23] describes a 'submicron metal cylinder with an asymmetric metal—insulator–metal tunnel junction at one end' to absorb and rectify light energy. Marks also proposed a system[24,25] in which a plastic film containing parallel chains of iodine molecules form linear conducting elements for the collection of optical energy. The theoretical conversion efficiency was claimed to be 72%[24] and a recently active but now expired web site[26] stated that the material was being actively developed.

Farber,[27] in addition to proving the concept of single-frequency microwave power reception by pyramidal dielectric antenna elements and rectification, attempted reception of light energy by SiC particles on modified abrasive paper. The results were, however, inconclusive, despite some electrical output being observed. This work was extended by Goswami *et al.*[14]

Kraus, in the second edition of his text,[28] proposed two orthogonally polarized arrays of λ dipoles, one array above the other on either side of a transparent substrate, with a reflector behind, to receive and rectify sunlight.

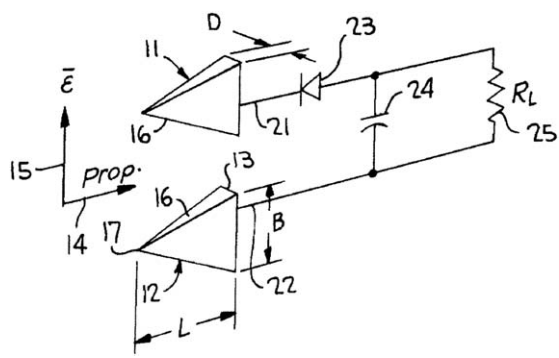

Figure 16.2 Electromagnetic wave energy converter proposed by Fletcher and Bailey. Reproduced from Bailey.[18]

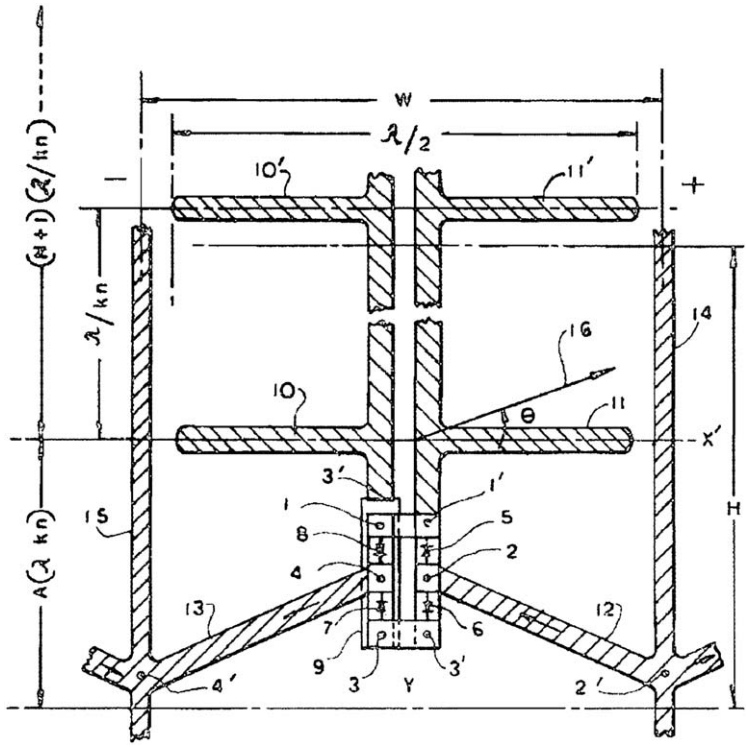

Figure 16.3 Marks' rectenna using array of dipoles and discrete rectifiers. Reproduced from Bailey *et al.*[19]

There is no mention there of any attempt to realize the device. Kraus stated that 100% aperture efficiency is, in principle, possible. A later textbook states that optical rectification is impractical because the diode electron relaxation time is too slow.[29]

Lin *et al.*[30] reported the first experimental evidence for light absorption in a fabricated resonant nanostructure and rectification at light frequency. The device used grooves and deposited metallic elements to form a parallel dipole antenna array on a silicon substrate and a p–n junction for rectification. They observed an output resonant with the dipole length and dependent on light polarization and angle of the incoming light, indicating that the device possessed antenna-like characteristics.

Berland *et al.*[31,32] undertook extensive development of theoretical and experimental models for optical antennas coupled to fast tunnel diodes, stating a theoretical efficiency for sunlight of up to 85%. They built model dipole rectenna arrays operating at 10 GHz, achieving over 50% conversion efficiency and integrated metal–insulator–metal (MIM) rectifier diodes into a μm-scale antenna.

Eliasson and Moddel proposed the use of metal/double-insulator/metal diodes for rectenna solar cells,[16,33] and demonstrated high responsivity at

60 GHz.[34] To circumvent *RC* time constant limitations of metal/insulator/metal diodes, the group proposed the use of traveling wave diodes[35,36] and graphene geometric diodes, which were demonstrated for infrared radiation.[37]

Wang *et al.*[38] made random arrays of aligned carbon nanotubes and demonstrated the polarization and length-dependence effects in the visible range.

Sarehraz *et al.*[39–41] focussed on the issues of skin effect in metallic antenna elements and the tiny voltage produced by each. Assuming a dipole structure, they calculate the available power and the efficiency of an MIM rectifier and DC power. Diode efficiency increases with input power and the authors conclude that, with their assumptions, about 5000 dipoles would need to feed each rectifier to exceed the efficiency of a silicon photovoltaic cell.

Corkish *et al.*[6] attempted to address the question of the theoretical limit on the efficiency of rectenna collection solar energy. They proposed combining concepts from classical radio-astronomical radiometry[42] with theories for rectification of electrical noise.[43] This work, like most preceding studies of solar rectennas, discussed a proposed extension of classical physical concepts, reliant on the Rayleigh-Jeans approximation and applicable for $hf(kT) \ll 1$. This approach is extended in the present chapter.

Kotter *et al.*[44] modeled, using a general Method-of-Moments software package, periodic arrays of square loop antennas for mid-infrared wavelengths and constructed devices. Modelling predicted a theoretical efficiency of 92% for antenna absorption of solar energy, with peak performance at 10 μm wavelength. Test devices were built on silicon wafers using electron beam lithography and prototype roll-to-roll printed arrays were produced. Peak operation for experimental devices was at 6.5 μm.

Osgood *et al.*[45] observed 1 mV signals from nanorectenna arrays of silver patterned lines coupled to NiO-based rectifier barriers illuminated by 532 nm and 1064 nm laser pulses and Nunzi[46] proposed reception by arrays of metallic, resonant nanoparticles and rectification by molecular diodes,[47] covalently linked to the antennas.

Eliasson[16] suggested that coherent illumination was required for rectennas to avoid cancellation of different components of the current, and that sunlight provides sufficient coherent only over a limited illumination area. Mashaal and Gordon[48] analyzed the coherence radius for broadband solar illumination.

Miskovsky *et al.*[49] proposed a sharp-tip geometry to rectify optical-frequency radiation to circumvent the *RC* time constant limitations of metal–insulator–metal diodes. Choi *et al.*[50] have presented a different approach to forming an asymmetric tunneling diode for high frequency rectification.

Gallo[51] proposed an innovative thermo-photovoltaic system in which the earth absorbs solar energy and the re-emitted thermal radiation is intercepted and converted by an infrared antenna array using printed gold square spirals. This could be of potential interest for stationary aerial platforms for earth observation, surveillance, etc. The antenna array was simulated at 28.3 THz (10.6 μm) for reception and rectification of circularly polarized plane

wave. As noted by Grover,[52] in accordance with the second law of thermodynamics the efficiency of such an approach depends on the antenna being at a significantly lower temperature than the earth and is likely to be very low in any conceivable implementation.

Grover *et al.*[53] rejected the use of classical approaches in favor of the semiclassical treatment of photon assisted transport, generalized for tunnel devices. They used this method to derive a piecewise-linear approximation to the current–voltage curve for an optical rectenna under monochromatic illumination. Using this treatment Joshi *et al.*[54] calculated the upper bound for rectenna solar cell conversion efficiency under broadband illumination.

Optical antenna structures, or antenna-coupled detectors, are under development for many actual and potential uses other than for solar energy collection.[4] In many of these other applications, issues discussed in this review as problems for implementation of antennas for energy collection can be seen as advantages. Small physical size, narrow bandwidth and polarization dependence can improve performance in many applications.[4] The research in this field has moved from infrared[55] devices to optical wavelengths as lithography technology has made smaller devices feasible. Here too, more tractable problems than solar energy rectification are commonly addressed. In particular, the difficult question of how to efficiently convert received energy to DC electricity does not always arise. Skigin and Lester[5] reviewed optical antennas under development for arrange of purposes, referring to dipole, bow-tie and Yagi-Uda styles. Antenna–load interactions at optical frequencies were investigated Olmon and Rashke.[3] They described the reception process by partitioning into three main steps: excitation of an antenna resonance by a freely propagating mode; its transformation into a nanoscale spatial localization; and near-field coupling to a quantum load. They suggested the necessary extension of antenna theory for the design of impedance-matched optical antenna systems coupled to loads. Vandenbosch and Ma[56] analyzed the upper bounds of the antenna efficiency for different metals in solar rectennas.

16.2.2 Wireless Power Transmission

Another potential application for rectennas is the wireless transmission of electrical power, either terrestrially or between satellites or between satellites and Earth.[57,58] Wireless power transmission is an old dream that is now commonly realized over short distances for battery charging in consumer and industrial devices. Interest in terrestrial wireless power transmission can be traced from Heinrich Hertz in the 19th century.[59] Nicola Tesla was one of the pioneers in its implementation with his experiments at Colorado Springs[60] at the beginning of the 20th century. W.C. Brown, at Raytheon Corp., led a long program of research into microwave power transmission with many technical successes for terrestrial, aerial and space applications, achieving efficiency of 84%.[59] The potential use of ground-based rectennas to collect microwave transmission from orbiting solar power stations has also attracted significant interest in recent decades.[57]

The problem being addressed in those studies is much simpler than that of solar energy reception and rectification since coherent radiation of a single polarization and frequency, commonly in the atmospheric window in the microwave band, may be chosen, excluding most of the more difficulties discussed below.

16.2.3 Radio-powered Devices

A range of low-power electronic devices has been developed to derive operating power from electromagnetic fields. The earliest radio receivers, crystal sets, were self powered by rectification of the incoming radio frequency signal. Several inventors have developed devices to monitor microwave oven leakage or other radiation by powering an indicator from the leaking radiation via a rectenna. A similar method has been used to power active biotelemetry devices, implanted therapeutic devices, radio frequency identification tags and transponders and even the proposed recharging of batteries in microwave ovens. Motjolopane and van Zyl[61] reviewed options for harvesting ambient microwave energy to supply indoor distributed wireless sensor.

16.2.4 Radio Astronomy

Radio astronomy technology provides, perhaps, the closest existing similarity to technology that might eventually permit antenna collection of solar energy and it might provide useful insights for future developments. The field of astronomy has a technological divide between optical and radio astronomy. Practitioners of the former rely on optical instruments such as lenses, reflectors and cameras. Radio astronomers share the extensive use of reflectors but antennas and radio receivers are the core components of radiotelescopes.[62] However, the two are likely to merge and overlap as the instrument technologies for each extend into the intervening gap. Radio astronomers routinely deal with broad bandwidth signals, a range of coherence and polarizations and, at the shorter wavelength end of their range of interest, components of small physical scale. They detect and measure black-body and/or other forms of radiation from celestial bodies, including the sun, but do not seek to maximize the extraction of energy.

16.3 Research Problems Concerning Rectennas for Photovoltaics

16.3.1 Fundamental Problems

16.3.1.1 Partial Coherence

In principle, it is possible to generate electrical power from purely incoherent photon sources, as this does not violate the second law of

thermodynamics. In fact non-coherent black-body radiation at an elevated temperature is equivalent to thermally agitated electromagnetic noise. Together with a heat sink, such noise at a higher colour temperature can contribute to DC electricity with the use of a rectifying heat engine. This conversion is limited by thermodynamic efficiencies, *i.e.* the Carnot efficiency or, more strictly, the Landsberg limit.[63] However, if sunlight is inherently partly coherent, higher efficiency figures may be achieved. In the field of traditional radio technologies, the rectification efficiency can even achieve 100% for purely coherent electromagnetic waves.

This consideration introduces a fundamental problem concerning the coherence properties of sunlight. Sunlight is normally regarded as incoherent radiation due to the nature of spontaneous emission. However coherence theory implies that even radiation emitted from incoherent sources still has equal-time partial coherence if the spatial separation is sufficiently small. Verdet[64] studied the coherence problem of sunlight for the first time. Since then researchers developed the van Cittert–Zernike theorem based on far-field assumptions.[65–67] Recently Agarwal *et al.*[68] used a different approach to study the partial coherence of sunlight, leading to expressions in good agreement with the far-field result.

The mutual coherence between two field points is defined by the equal-time mutual coherence function (EMCF),[48] which is the statistical time average of the product of the field at the two positions (Figure 16.4), *i.e.* $\langle \boldsymbol{E}^*(\boldsymbol{r}_1)\boldsymbol{E}(\boldsymbol{r}_2)\rangle$. From the treatment by Agarwal *et al.*, for simplicity, a scalar field U (as one component of $\boldsymbol{E}$) is used instead of the vector electric field E. The time-dependence of this field is converted into the frequency domain by Fourier transformation, enabling the possibility of dealing with the wide spectrum of sunlight. The mutual coherence is characterized by a cross-spectral density function instead:

$$W(\boldsymbol{r}_1,\boldsymbol{r}_2,\omega) \equiv \langle U^*(\boldsymbol{r}_1,\omega)U(\boldsymbol{r}_2,\omega)\rangle \tag{16.1}$$

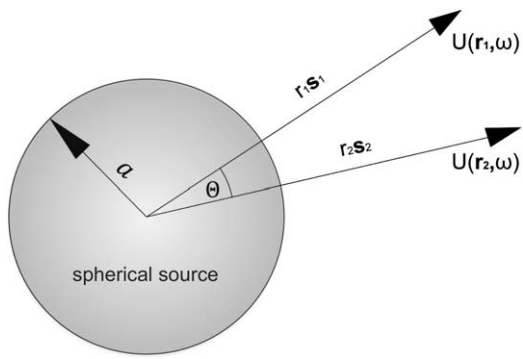

Figure 16.4 Schematic diagram for two light rays emitted from a spherical source. Reproduced from Agarwal and Wolf.[68]

This scalar field, U, as a solution of the scalar Helmholtz equation, can be expanded into a series of spherical harmonics:

$$U(\boldsymbol{r},\omega)=\sum_{lm}c_{lm}h_l^{(1)}(kr)Y_{lm}(\theta,\phi) \tag{16.2}$$

where $h_l^{(1)}$ is the spherical Hankel function of the first kind and Y_{lm} denotes the spherical harmonics. $k=2\pi/\lambda=\omega/c$ is the wave-vector of the monochromatic light. θ and ϕ denote the angular coordinates of the field point. The coefficients c_{lm} are random, depending on the statistical properties of the field on the surface of the light source. The cross-spectral density is then expressed by Equation (16.3) after substituting Equation (16.2) into Equation (16.1):

$$W(r_1,r_2,\omega)=\sum_{lm}\sum_{l'm'}c_{lm}^{*}c_{l'm'}h_l^{(1)*}(kr_1)h_{l'}^{(1)}(kr_2)Y_{lm}^{*}(\theta_1,\phi_1)Y_{l'm'}(\theta_2,\phi_2) \tag{16.3}$$

The next step is to include appropriate boundary conditions for Equation (16.3). Considering the fields at the surface of the spherical source, its cross-spectral density is delta-function correlated:

$$W(as_1,as_2,\omega)=I_0(\omega)\delta^{(2)}(S_2-S_1) \tag{16.4}$$

where $\boldsymbol{s}_1$ and $\boldsymbol{s}_2$ are the respective unit vectors in the directions of the vectors $\boldsymbol{r}_1$ and $\boldsymbol{r}_2$ and $I_0(\omega)$ is the effective intensity of the field on the spherical surface of the source. $\delta^{(2)}$ is the two-dimensional Dirac delta function with respect to the spherical coordinates (θ,ϕ). This delta function can be expanded according to the spherical harmonic closure relation:

$$\delta^{(2)}(\boldsymbol{s}_2-\boldsymbol{s}_1)=\sum_{lm}Y_{lm}^{*}(\theta_1,\phi_1)Y_{lm}(\theta_2,\phi_2) \tag{16.5}$$

The boundary condition, Equation (16.4), attributes the physical origin of the partial coherence of sunlight to the geometric correlation at the spherical surface of the light source. By matching Equation (16.3) to the boundary condition, the correlation function of c_{lm} is found to be:

$$\langle c_{lm}^{*}c_{l'm'}\rangle=\delta_{ll'}\delta_{mm'}\frac{I_0(\omega)}{|h_l^{(1)}(ka)|^2} \tag{16.6}$$

where $\delta_{ll'}$ and $\delta_{mm'}$ are the Kronecker delta functions. By using the spherical harmonic addition theorem the cross-spectral function takes its final form:

$$W(\boldsymbol{r}_1,\boldsymbol{r}_2,\omega)=\sum_{l}\frac{2l+1}{4\pi}\frac{I_0(\omega)}{|h_l^{(1)}(ka)|^2}h_l^{(1)*}(kr_1)h_{l'}^{(1)}(kr_2)P_l(\cos\Theta) \tag{16.7}$$

where Θ is the angle between $\boldsymbol{r}_1$ and $\boldsymbol{r}_2$. P_l is the Legendre polynomial of order l.

The angular dependence of the degree of coherence is obtained by setting $r\equiv r_1=r_2$, and then normalizing $W(\boldsymbol{r}_1,\boldsymbol{r}_2,\omega)$ according to its peak value (at $\Theta=0$). The numerical results (Figure 16.5) show that the angular spread

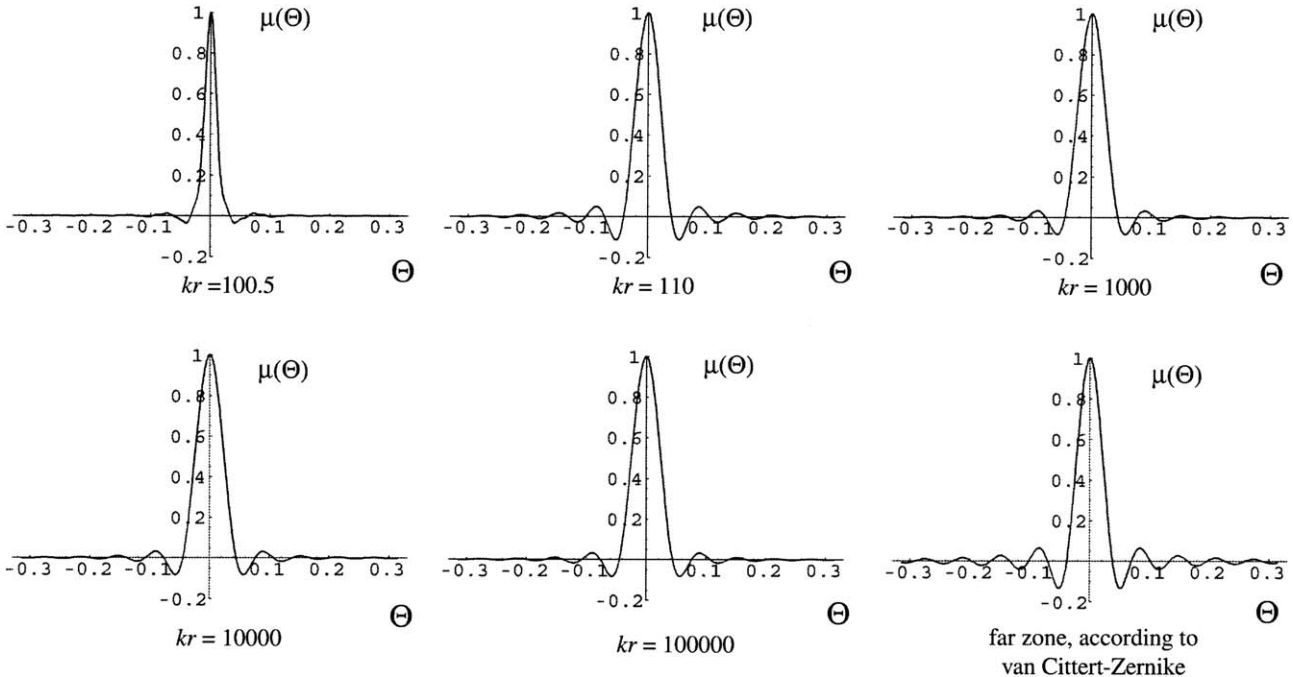

Figure 16.5 Degree of coherence with different angular distances between two field points. Each figure corresponds to a specified radial distance to a spherical source whose radius is kr = 100.
Reproduced from Agarwal and Wolf.[68]

of the coherence remains a constant when the field points are more than a few wavelengths away from the source. This confirms that the far-field relation also applies to field points essentially within the near-field regime.

Figure 16.5 also provides a comparison between the expression derived by Agarwal and Wolf[68] and the traditional far-field van Cittert–Zernike theorem:

$$W(r\boldsymbol{s_1}, r\boldsymbol{s_2}, \omega) = \frac{J_1[2ka\sin(\Theta/2)]}{ka\sin(\Theta/2)} \tag{16.8}$$

where Θ is still the angular distance between the unit vectors $\boldsymbol{s_1}$ and $\boldsymbol{s_2}$ and J_1 is the Bessel function of the first kind and order 1. Numerically, this expression in a very good agreement with the general relation derived here, enabling us to analyze the coherence problem simply with the van Cittert–Zernike relation.

The previous analysis gives expressions for the degree of coherence at a quasi-monochromatic spectrum. To convert the whole spectrum of sunlight by the rectenna system, the partial coherence of the broadband radiation requires investigation. Mashaal and Gordon[48] have provided a quantitative analysis. In their treatment, the far-field van Cittert–Zernike theorem is represented in terms of the solar angular radius Φ and the intensity, I (per solid angle of black-body radiation from the sun):

$$\langle \boldsymbol{E}^*(r_1,\omega)\cdot\boldsymbol{E}(r_2,\omega)\rangle = \pi\Phi^2 I\frac{J_1[2ka\sin(\Theta/2)]}{ka\sin(\Theta/2)} \approx \pi\Phi^2 I\frac{J_1(k\Phi|r_1-r_2|)}{k\Phi|r_1-r_2|/2} \tag{16.9}$$

where r_1 and r_2 denote the field point positions in the transverse direction. For a circular antenna placed transverse to the incident sunlight, the maximum separation between r_1 and r_2 is the antenna diameter, $2b$. The whole-band equal-time mutual coherence function (EMCF) is simply an integration of the quasi-monochromatic EMCF, as the coherence between waves of different frequencies always drops to zero:

$$\langle \boldsymbol{E}^*(r_1)\cdot\boldsymbol{E}(r_2)\rangle = 2\pi\Phi^2\int_{\lambda_{min}}^{\lambda_{max}} I_{BB}(\lambda)\frac{J_1(k\Phi|r_1-r_2|)}{k\Phi|r_1-r_2|/2}d\lambda \tag{16.10}$$

where the spectrum of black-body radiation is:

$$I_{BB}(\lambda) = 2hc^2/\lambda^5\cdot[\exp(hc/kT\lambda)-1]^{-1} \tag{16.11}$$

The average power intercepted by the antenna is:[48]

$$\langle P\rangle = \frac{1}{A_{ap}}\int_{A_{ap}}\int_{A_{ap}}\langle \mathrm{E}^*(\mathrm{r}_1)\cdot\mathrm{E}(\mathrm{r}_2)\rangle dAdA' = \int_{\lambda_{min}}^{\lambda_{max}} I_{BB}(\lambda)\lambda^2\left[1-J_0^2(k\Phi b)-J_1^2(k\Phi b)\right]d\lambda \tag{16.12}$$

where the integrations are over the antenna's full aperture area A_{ap}. From Equation (16.12) the intercepted power is proportional to the aperture area (πb^2), *i.e.* $\langle P\rangle = \pi^2\Phi^2 b^2 I$, if the antennas size is sufficiently small, ($k\Phi b \ll 1$).

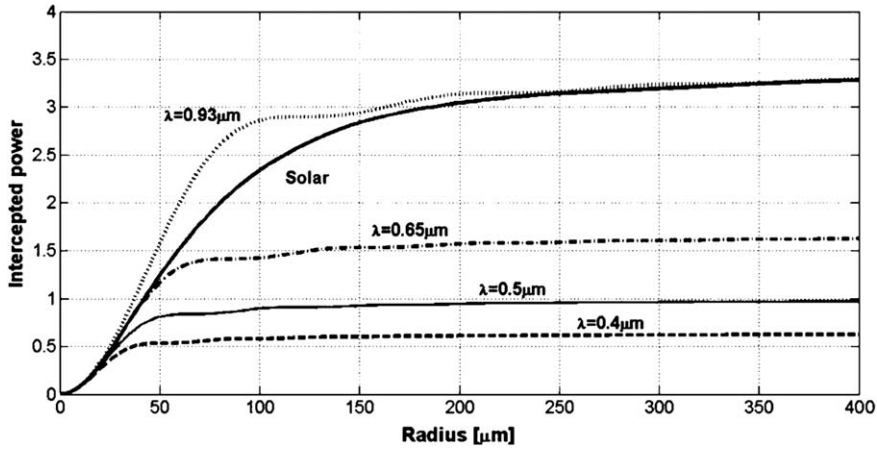

Figure 16.6 Intercepted power (normalized to the asymptotic value for $\lambda = 0.5$ μm) as a function of detector radius. For each curve the asymptotic power is $\overline{\lambda^2}I$, while at small radius, all curves converge to the result for coherence of $\pi^2\Phi^2b^2I$.
Reproduced from Mashaal and Gordon.[48]

This corresponds to the case of pure-coherent interception. On the other hand, the pure-incoherent limit exists for large antennas, ($k\Phi b \gg 1$). At this limit the intercepted power does not increase with the antenna size ($\langle P\rangle = \overline{\lambda^2}I$), as it is restricted by the partial coherence of sunlight. Figure 16.6 illustrates the increase of intercepted power with the antenna radius. When the antenna radius exceeds approximately a hundred times of the wavelength, the intercepted power gradually levels off.

Coherence efficiency can be defined as the ratio of the intercepted power to its value at the pure-coherence limit ($\pi^2\Phi^2b^2I$). This efficiency provides a measure of the loss of collectible power due to the incoherence of sunlight. Figure 16.7 provides the coherence efficiency for whole-spectrum sunlight, as a function of the antenna radius. A 90% coherence efficiency can be achieved with a radius of 19 μm.

16.3.1.2 Polarization

Most traditional antennas only accept a single linear or a single circular polarization, which is insufficient to match the unpolarized nature of directly incident sunlight. Such antennas can at maximum absorb 50% of the total radiation. To overcome this problem, cross-polarized structures have been designed as a combination of two linear or circularly polarized antennas placed orthogonally. With these structures it is possible to provide a 100% aperture efficiency in principle.[28] Prior splitting of sunlight into two orthogonal linearly or circularly polarized components, by use of birefringent crystals for example, would be necessary for some possible converter designs, such as Song's ratchets.[69]

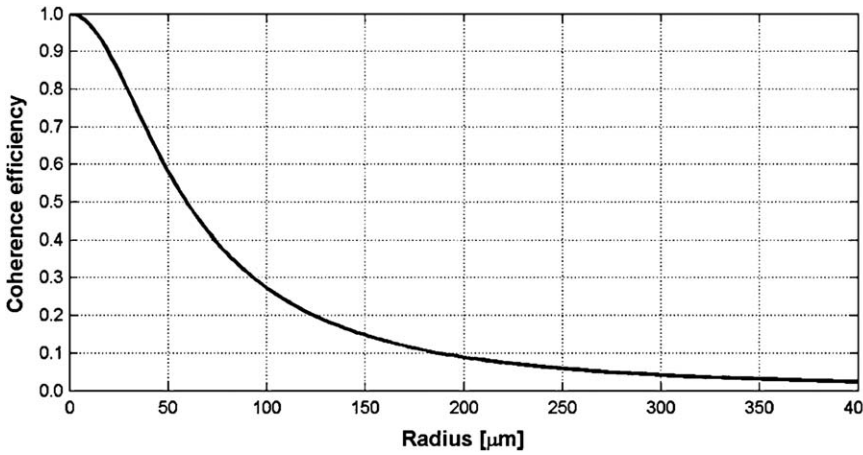

Figure 16.7 Coherence efficiency (intercepted power relative to its value in the pure-coherence limit) as a function of antenna radius for solar radiation. Reproduced from Mashaal and Gordon.[48]

Another practical design adopts a unidirectional conical four-arm form that is effectively two intertwined antennas for both polarizations (Figure 16.18). This sinuous antenna can produce power outputs for either the two linear or the two circular polarizations. It also provides a large bandwidth. None of the frequency-independent antenna designs are very directive (*i.e.*, they are restricted to low solar concentration ratios) but it would be feasible to use them as feed antennas for concentrating reflectors or lenses.[70]

16.3.1.3 Bandwidth

The broadband nature of sunlight limits the possibility of accepting its energy by a single antenna. In fact, 60% of the solar spectrum is contained in a fractional bandwidth of 60%.[39] On the other hand, a fractional bandwidth of 15–20% is usually regarded as wide bandwidth for conventional microwave antennas, presenting a problem for the application of antenna techniques to solar power harvesting.

Radio antenna designs, termed 'frequency independent', have been devised to achieve greater bandwidths,[71] but their complexity clearly presents a challenge for fabrication at the scale required for optical reception. In order to make an antenna independent of frequency it is necessary to ensure that the antenna's radiating structures are specified by angles only and to be truly frequency independent, an antenna would need to infinite in size and its feed point would need to be infinitely fine. In practice, antenna engineers can obtain up to 100:1 bandwidth. Multi-arm planar spiral antennas are frequently used to obtain the required frequency range but, undesirably in our case, have radiation lobes on either side of the substrate plane.

Attachment to a transparent dielectric substrate or lens would allow radiation to be better received through the substrate side. Conical spiral antennas (Figure. 16.8), 3D structures with spiral arms wrapped over the surface of a cone, concentrate the radiation pattern in the direction of the cone apex, demonstrating a 10:1 bandwidth.[71] Planar spiral antennas have been made, with lenses, in the THz range[26] but the current authors have not identified examples of infrared or optical conical spiral antennas.

Another design of wide bandwidth antenna[28] is a planar version of the exponential horn antenna (Figure 16.9), which has the advantage of being compatible with printed-circuit fabrications. The horn takes the form of an exponential notch in the conducting surface of a circuit board, and couples to a 50 Ω strip line on the other surface of the board. It can achieve a bandwidth of 5:1, which is still far from the requirement for whole-band sunlight absorption.

Apart from the difficulty of fabricating a frequency-independent antenna for optical wavelengths, the introduction of harmonics is another important issue. These harmonics, allowed by the wide bandwidth, make it more difficult to achieve high rectification efficiency.[6] Furthermore, an optical rectenna operating with terrestrial sunlight intensities cannot efficiently convert the entire solar spectrum,[54] as discussed later in this chapter.

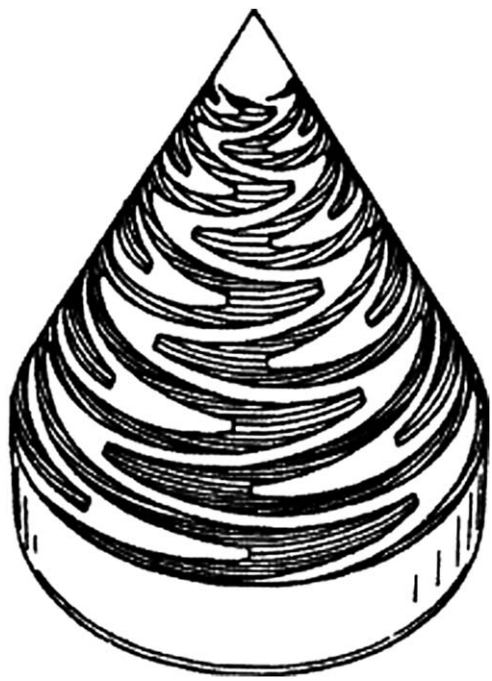

Figure 16.8 Conical sinuous, dual-polarized antenna. Reproduced from DuHamel and Scherer.[70]

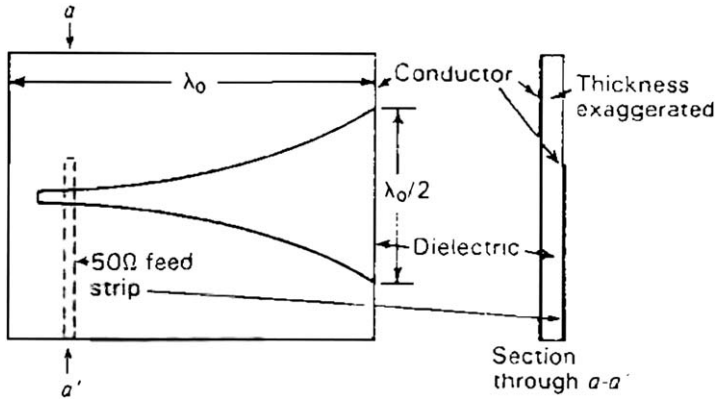

Figure 16.9 Exponential notch broadband antenna with 50 Ω microstrip feed. Reproduced from Kraus.[28]

However, in practice, it is both infeasible and unnecessary to accept the whole solar spectrum using a single antenna. A practical solution may be to absorb sunlight using an approach that resembles the operation of a tandem solar cell. With this approach different rectennas in optical series are used to split the whole spectrum of sunlight and contribute to the power output collectively. Unlike spectral splitting in conventional solar cells, where different materials are required for each spectral range, spectral splitting can be accomplished in rectenna solar cells simply be selecting different operating voltages for each spectral range,[54] along with an appropriately sized antenna. This allows the adoption of narrow-bandwidth antennas. In fact even if each individual antenna has a fractional bandwidth of 20% (typical figure for traditional microwave antennas), only 11 antennas are required to cover the whole wavelength range (0.2–2 μm) of sunlight.

16.3.2 Practical Problems

16.3.2.1 Element Size

Unlike the commonly used microwave antennas that are of one-half the wavelength of the incident light, optical antennas at resonance may have different lengths from that predicted by classical antenna theory. Mühlschlegel *et al.*[7] found that the length of optical antennas at resonance is considerably shorter than one-half the wavelength, if accounting for the finite metallic conductivity at optical frequencies. The excitation of plasmon modes at optical frequencies also plays a fundamental role in this. As demonstrated by Podolskiy, optical excitation of surface plasmons results in strong local field enhancement if the antenna length is around one-half of the plasmon wavelength.[72] These surface plasmons have much shorter wavelengths than free-space radiation at optical frequencies, contributing to a shorter antenna length at resonance. Mühlschlegel *et al.*[7] demonstrated

that nanometer-scale gold dipole antennas at resonance, with an optimal antenna length of 255 nm, led to white-light supercontinuum generation. This scale is far below the coherence limit of sunlight so that the incoherence during rectification is no longer an issue.

The dimension of the rectification component is limited by its ultrafast response speed at optical frequencies. Conduction electrons interacting with the electromagnetic field of a coherent light simultaneously undergo two motions.[73] We are interested in estimating the magnitude of the transverse oscillation at optical frequencies. Semchuk *et al.*[73] obtained an expression, valid for non-relativistic motion, for the amplitude of the transverse oscillation:

$$x_{max} = \frac{qE_0}{4\pi^2 f^2 m} \tag{16.13}$$

where f and E_0 are the frequency and the peak amplitude of the external field, respectively and m is the electron mass. This leads to a restriction on the maximum excursion of the electron from its equilibrium position:

$$x_{max} \ll \frac{c}{2\pi f} \ll \frac{\lambda}{2\pi}$$

For light of wavelength 500 nm this results in an amplitude of several nanometers and places a restriction on the dimensions of the structures that could be used as rectifying elements. The most popular option of the high-frequency rectifier is the metal–insulator–metal (MIM) diode, which is under intensive investigation. Such structures need to be extremely thin, *i.e.* several nanometers, partly because the current needs to be sufficiently high to provide a low impedance to match that of the antenna for efficient power coupling.[74]

16.3.2.2 Rectifier Speed

It is a challenging task to rectify electric signals with optical frequencies. The frequency limit of Schottky diodes is in the far-infrared region,[74] beyond which the responsivity drops quickly. The conventional p–n junction diode has an even worse response to high frequencies. In fact the oscillation period for optical frequencies (600 THz is the centre of the visible window) is around 1/600 THz = 1.7 fs. This time scale is even shorter than the electron relaxation time,[77] which implies that any rectification relying on diffusive transport of carriers would be not fast enough to respond to optical frequencies.

However, there are no fundamental restrictions on the feasibility of using rectifiers that rely on quantum transport. A promising option is the metal–insulator–metal (MIM) diode. The nanometer-scale insulator layer sandwiched between two metal layers works as a potential barrier, allowing electrons to tunnel through under positive bias. When the diode is

negatively biased, the conduction band of the insulator becomes flat, contributing to a large effective barrier thickness. This blocks the transport of electrons as an exponential function of the voltage.

Grover has pointed out that a severe problem preventing existing MIM diodes to be applied to solar energy conversion is the limitation of its *RC* time constant.[74] Even for extremely low resistance MIM diodes, the *RC* time constant, which we desire to be below 1 fs, is still too long for visible frequencies. This analysis puts a limit for parallel plate diodes, though it might be overcome by other potential technologies. Within the regime of quantum transport, each planar mode can carry at maximum a conductance quantum, *i.e.* $(12.9\ \mathrm{k\Omega})^{-1}$ with spin degeneracy included.[74] If the diode consists of a solid with a planar periodicity of ~ 5 Å, the density of planar modes would be around $1/(5\text{Å})^2 = 4\times10^{18}\ \mathrm{m}^{-2}$. If electrons of these modes always have complete transmission, the resistance is $12.9\ \mathrm{k\Omega}/4\times10^{18}\ \mathrm{m}^{-2} = 3.2\times10^{-15}\ \Omega\ \mathrm{m}^2$. To estimate the capacitance of the diode, we consider a scenario: a short separation of 1nm for ballistic transport, and a material permittivity of 10. This gives a capacitance of $\sim 0.1\ \mathrm{F\ m}^{-2}$ and hence a *RC* constant of $\sim 10^{-16}$ s. This sets a fundamental limit for the minimal *RC* value one could ever get. It does not change with the diode area and is shorter than the time scale of visible frequencies. This topic is further discussed, with a different approach, in section 16.7.1.1.

16.3.2.3 Filtering

The rectenna technology has been intensively investigated for converting microwave into DC energy.[75–77] The frequency range of these studies is from 1 GHz to 10 GHz, much lower than visible frequencies. However, their general design structures might still potentially apply to rectennas operating at higher frequencies. A common idea is that a rectenna should include an input filter before the rectifier and an output filter after the rectifier (Figure 16.1).

The input filter can be a band-pass filter[76] or a lowpass filter.[77] Both the input filter and the output filter are used to store energy during the off period of the diode. It was found that power flow continuity was able to be achieved, even with half-wave rectification, by suitable filter design.[78]

More importantly, the input filter restricts the flowing-back and re-radiation of high-frequency harmonics generated by the rectifier. By correctly setting the *RC* time constant of the input filter, it allows the fundamental to pass without much attenuation, while rejecting all the harmonics. Computer simulation has revealed that the power loss due to harmonics generated by the diode is significant, especially when a resonant loop forms between the diode and transmission lines at a harmonic frequency.[77]

For collection of broadband sunlight, there is an additional problem as the harmonics generated by rectification of long-wavelength light can have frequencies within the desired bandwidth for energy acceptance. In fact the solar spectrum has a frequency range from 150 THz to 1500 THz, being

wide enough to allow harmonics to pass. It will become necessary to split the spectrum and direct different fractions to different rectennas. Another possible method is to use a stack of rectennas, each comprising two orthogonally oriented arrays. Unlike a tandem photovoltaics stack, which effectively works as a series of high-pass filters, the rectennas are arranged in an increasing order of operating frequency, if their input filters are low-pass.

The output filter is basically a DC filter, aiming to block AC power from reaching the load, where it would be lost as heat. It was found that the distance between the rectifier and the output filter might be used to cancel the capacitive reactance of the diode, which is needed to maximize the diode efficiency.[75]

Although the rectenna structure and the filters can be fabricated using conventional transmission-line technology, there is trend in the microwave region of using microstrip-printing techniques.[75,76] In the design by McSpadden *et al.*[75] the output filter is a RF short chip capacitor, while the low pass filters are strips printed on the opposite side of the substrate, as they require a much lower capacitance (Figure 16.10).

16.3.2.4 Element Matching

There are two types of matching problems for rectenna-based solar energy conversion. The first is to match the characteristics of components within one rectenna circuit in order to obtain the maximum conversion efficiency, while the second is to combine the power from different rectenna circuits for a useful DC voltage.

Impedance matching between the antenna and the diode forms the most important of the matching problems. Mismatch between components can lead to reflection or re-radiation, rather than absorption of power. Especially

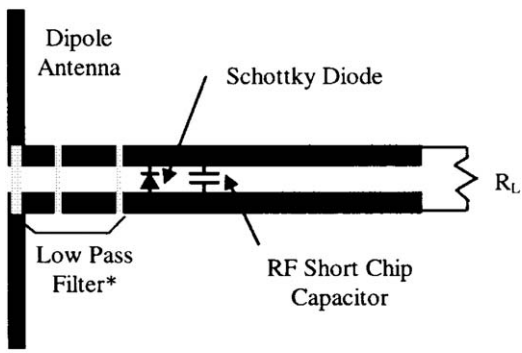

Figure 16.10 Microwave printed rectenna element. The dipole antenna and transmission line are printed on one side of the substrate and the low-pass filter is formed by strips printed on the opposite side. Reproduced from Semchuk *et al.*[75]

when there is a lack of input filters, the non-linear nature of the rectifier generates significant re-radiation of harmonic frequency energy.[79] The simplest case of rectifying monochromatic radiation is discussed in the following content.

The small-signal circuit model is illustrated in Fig. 16.11. The antenna, as a receiver, is modeled as an ac voltage source $V\cos\omega t$ with an internal resistance, R_A.[74] A resistor and a capacitor connected in parallel represent the differential resistance R_D and the junction capacitance C_D of the diode.

The voltage across the rectifier includes a DC component v_r, as the result of the rectification process, and an ac component v_{ac}, which involves the fundamental transmitted from the antenna and the harmonics generated from its non-linearity. To model the rectifier, consider the Taylor expansion of its *I–V* characteristic in the neighborhood of v_r:

$$I(V) = I(v_r) + I'(v_r)v_{ac} + \frac{I''(v_r)}{2}v_{ac}^2 + O(v_{ac}^3) \tag{16.14}$$

The ac component is assumed to be so small that the higher-order term $O(v_{ac}^3)$ is regarded as negligible. Using time-averaging technique, the rectified current i_r and the power dissipated in the diode are retrieved:

$$i_r = \langle I \rangle = I(v_r) + \frac{I''(v_r)}{2}\langle v_{ac}^2 \rangle \tag{16.15}$$

$$P_r = \langle Iv \rangle \approx i_r v_r + I'(v_r)\langle v_{ac}^2 \rangle \tag{16.16}$$

It is noted that the differential resistance $R_D = 1/I'(v_r)$. From Equation (16.15) and Equation (16.16) we can define the responsivity of the rectifier as:

$$\beta(v_r) = \frac{i_r - I(v_r)}{P_r - i_r v_r} = \frac{1}{2}\frac{I''(v_r)}{I'(v_r)} \tag{16.17}$$

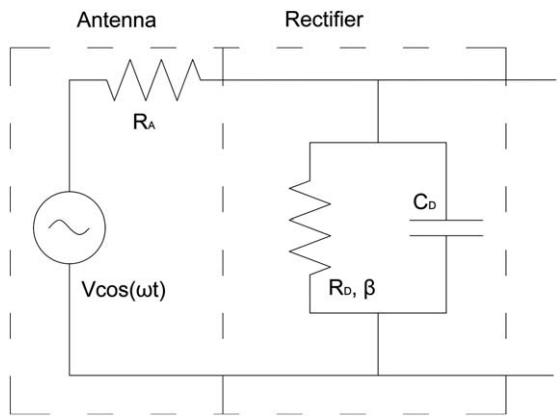

Figure 16.11 Small-signal circuit model of the rectenna. Adapted from Podolskiy *et al.*[74]

The responsivity of a diode reflects its ability to rectify current. It is a constant depending on the material and structure of the rectifier. Detailed circuit analysis on the rectenna system gives expression for the overall conversion efficiency:

$$\eta = \beta^2 P R_A \left\{ \frac{4R_A R_D / (R_A + R_D)^2}{1 + [\omega R_A R_D / (R_A + R_D) C_D]^2} \right\}^2 \frac{R_A R_D}{(R_A + R_D)^2} \tag{16.18}$$

The dimensionless term inside the braces is defined as the coupling efficiency, η_C. Its numerator has the same form as the term behind the braces, reaching its maximum when $R_D = R_A$. This corresponds to the condition of impedance matching between the rectifier and the antenna. The denominator has its minimum value at $\omega(R_A \| R_D)C_D = 0$. For RC value increases above the time period of the incident light, the overall efficiency drops quickly.

A typical antenna for microwave purposes has an effective impedance of around 100 Ω. This scale of resistance is hard to achieve for the rectifier, unless the junction capacitance is sacrificed.[52] This problem might be avoided by operating the rectenna with a load of low resistance and low capacitance.

With respect to matching aspects of the methods of combining power from different antennas, two basic families of designs have been proposed. Bailey, for example, had individual pairs of antenna elements each supplying its own rectifier and the DC rectifier outputs were combined.[18] Kraus, for example, on the other hand, combined the electrical oscillations from many antenna elements in a particular phase relationship and delivered their combined output to a rectifier.[28] With the former method there is the immediate concern that the tiny power expected from one or two antenna elements may not be enough to produce sufficient voltage to allow proper operation of any conceivable rectifier diode. The latter approach overcomes that problem but at the expense of the need for spatial coherence across all the antenna elements feeding a rectifier. In fact the micro-scale coherence limit for sunlight allows the combination of coherent power from a few nano-scale antennas. In addition, Kraus' suggested antenna structure is not sufficiently broadband for the light spectrum.

16.3.2.5 Materials/Skin Effect

The ac current density in a conductor decreases exponentially from its value at the surface due to the so-called skin effect:

$$J = J_S e^{-d/\delta} \tag{16.19}$$

The skin depth δ characterizes the effective thickness of the surface region that conducts ac currents. It is frequency-dependent according to Equation (16.26):[80]

$$\delta = \sqrt{\frac{2\rho}{\omega\mu}} \sqrt{\sqrt{1 + (\rho\omega\epsilon)^2} + \rho\omega\epsilon} \tag{16.20}$$

This equation is valid at least up to microwave frequencies. In this frequency range, metallic materials have the relation $\delta \propto \sqrt{1/\omega}$ as $\rho\omega\epsilon \ll 1$. Assuming the skin depth is much smaller than the diameter of the transmission line, the skin depth and, hence, the conductance drops by a factor of 1/10 000 if increasing the frequency from 60 Hz to 6 GHz, which is still far below optical frequencies. This would lead to a significant resistive loss for optical rectennas.

As the time periods of optical frequencies are comparable to or even shorter than the electron relaxation time, Equation (16.20) requires modification due to the ballistic nature of electron transport. Nevertheless, the resistance continues to increase with frequency rise due to the skin effect. Sarehraz *et al*. have indicated that silver at optical frequencies has a skin depth of only 2–3 nm and a resistance of 5–7 Ω per square.[39]

The skin effect[56] can be controlled by replacing metallic materials with dielectrics. If assuming the skin depth δ is much smaller than the wire diameter D, the resistance R is:

$$R = \frac{L\rho}{\pi D\delta} = \frac{L}{\pi D}\left\{\sqrt{\frac{\rho\omega\mu}{2}}\left[\sqrt{\sqrt{1+(\rho\omega\epsilon)^2}+\rho\omega\epsilon}\right]^{-1}\right\} \tag{16.21}$$

where L denotes the length of the wire. The minimal value of the material-dependent term in the braces can be achieved if the resistivity ρ and the permeability, μ, of the material are both small while the permittivity, ϵ, is as large as possible. For optical frequencies ($\sim 10^{15}$ Hz), the term $\rho\omega\epsilon$ is comparable to 1. This indicates that an increasing permittivity ϵ begins to significantly decrease the resistance ($\sim \epsilon^{-0.5}$) while the material resistivity ρ becomes less relevant. Low resistivity dielectrics could thus potentially benefit the solar application of rectennas.

Another approach is to optimize the geometric design of the antenna. A large surface area is required, which gives advantages to planar rather than wire antennas. Apart from the antenna, other components of the rectenna, including the rectifier and the filters, also requires optimization in order to avoid high resistances.[39]

16.4 Thermodynamics of Rectennas

Strictly speaking the rectenna system is not a thermodynamic system as the excited plasmon polaritons do not equilibrate. In fact at least for microwave frequencies the excitation retains the same spectral density as the incident light. In addition, the spatial coherence of the sunlight makes it possible to have coherent signals, which are different from thermal emissions.

However, in some special cases the excited plasmons can have the spectral density of an equilibrated distribution, *i.e*., Bose–Einstein statistics. In this situation, with the assumption that partial coherence of incident light is

weak, the incident light excites ac signals in the antenna that simulate thermal noise. A thermodynamic analysis can thus improve our understanding on the limitation of such solar energy converters.

16.4.1 Broadband Antenna Modeled as a Resistor

The thermal noise, or the Johnson–Nyquist noise, of a resistor, originates from the thermal agitation arising from electromagnetic energy. This electrical energy is like white noise, with evenly distributed components at all frequencies. Although the power accepted by the antenna and the thermal noise of a hot resistor seem unrelated, they in fact share common properties. A simple way to interpret this is to consider the thermal emission from a hot resistor. The emission, originated from the Johnson–Nyquist noise, has similar properties to black-body radiation.

Following this philosophy, Dicke described a thought experiment in 1946, leading us to the formulae for the voltage excited in the antenna.[42] In Figure 16.12 the antenna is bathed in background radiation emitted from a black-body at temperature T. Regardless of other energy losses, the radiation emitted from the black-body can be either reflected or accepted by the antenna. The antenna is assumed to have effective impedance matched with the transmission line, and the resistive load at the other end of the circuit matches the transmission line too. The whole system is at the same temperature T and is isolated from the environment. This allows detailed balance of the energy transfer between the black-body and the circuit. According to the transmission line theory, the power flowing to the load is not reflected back for the impedance matching configuration. On the other hand, the thermally agitated voltage generated across the resistive load feeds energy back to the antenna for re-emission. These two powers are equal to each other, enabling the substitution of the antenna with a resistor of the antenna's effective impedance (Figure 16.12).

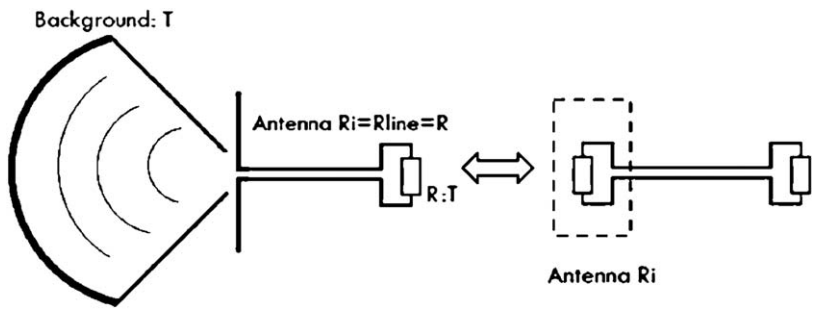

Figure 16.12 An impedance-matched antenna-resistor system bathed in black-body radiation. The thermal equilibrium between the background and the resistor ensures the balance of two powers flowing in opposite directions. The background radiation plus the antenna is thus equivalent to the hot resistor.

A more strict proof of this equivalency is provided as below in terms of their spectral densities. Due to the non-reflecting property of this circuit configuration, the power flowing into the load P_R equals to the power intercepted by the antenna:

$$P_R = \int \frac{1}{2} \frac{\Omega \cdot A_{eff}}{4\pi^3 c^2} \frac{\hbar\omega^3}{e^{\hbar\omega / kT} - 1} d\omega \tag{16.22}$$

The integration is over the whole spectral range of the radiation. Ω and A_{eff} denote the acceptance solid angle and the effective aperture area of the antenna, respectively. The 1/2 term accounts for the fact that the antenna can only intercept one polarization and, thus, absorb only half of the incident power. The rest of the integrand is simply the Planck's equation for the black-body radiation. According to the antenna theory, there is a general relation between the acceptance solid angle and the effective area:

$$\Omega \cdot A_{eff} = \lambda^2 \tag{16.23}$$

where λ is the wavelength of the radiation. By applying this relation to Equation (16.22), the frequency dependence of the integrand changes from ω^3 to ω. This is essentially because the density of electromagnetic modes changes its form from three-dimensional to one-dimensional. If regarding the antenna as a voltage source v_a, the power dissipated by the load is equal to the power absorbed by the antenna:

$$P_R = \int \frac{1}{2\pi} \frac{\hbar\omega}{e^{\hbar\omega / kT} - 1} d\omega = \int \frac{\langle v_a^2 \rangle_\omega}{4R} d\omega \tag{16.24}$$

This indicates that the voltage component (in a frequency range from ω to ω + dω) excited by the antenna absorbing the black-body radiation at temperature T is:

$$\langle v_a^2 \rangle_\omega = \frac{2}{\pi} \frac{R\hbar\omega}{e^{\hbar\omega / kT} - 1} \tag{16.25}$$

At the low frequency limit, *i.e.*, $\hbar\omega \ll kT$, there is an approximate expression $\langle v_a^2 \rangle_\omega \approx 2/\pi \cdot kTR$ or $\langle v_a^2 \rangle_f \approx 4kTR$. This is exactly the expression for the spectral density of the Johnson–Nyquist noise.

As a conclusion, an antenna with ideal broadband absorption can generate voltages with the spectral density of the thermal noise across a hot resistor. The thermal noise is at the temperature of the incident black-body radiation, and is excited across a resistor of the antenna's effective impedance. It is noted that for an antenna with incomplete absorption, the excited frequency-dependent voltage is scaled down by the antenna's absorptivity. However, unlike the Johnson–Nyquist noise, which is purely incoherent, the information of partial coherence can be retained in the excited ac voltage.

16.4.2 Energetics of Thermal Rectification

From the previous section, the solar radiation plus the ideal broadband antenna can be substituted by a hot resistor at a fixed temperature, T_C. Thus the rectification process can now be considered as for the thermal noise generated by a hot resistor,[6] with the assumption of complete incoherence. In this section thermal rectification by a cold diode is considered, providing a quantitative picture for the rectenna system.

We assume that the antenna is ideal, *i.e.*, it converts all power into radiation. The equivalent circuitry is shown in Figure 16.13(a), representing a thermal converter between the resistor (heat source) at temperature T_C and the diode (heat sink) at temperature T_A. This converter rectifies Johnson–Nyquist noise generated across the hot resistor and extracts a DC current, i, through the load. It is noted that the hot resistor, R, shown in Figure 16.13(a), which represents the antenna accepting sunlight, is replaced by a noiseless resistor R and an AC voltage source v(t) in Figure 16.13(b). The capacitor C is the output filter for generating a DC voltage $\langle u(t)\rangle$ across the load.

For the purpose of circuit analysis, the hot resistor is replaced by a noiseless resistor and a voltage source v(t) connected in series (Figure 16.13(b)). The correlation between v(t) and the voltage across the load, u(t) will be revealed in the following analysis.

Corresponding to the absorption of the antenna, the power supplied from the voltage source is:

$$S_R = \langle v(t) i_R(t)\rangle = \langle v \cdot (v-u)/R\rangle = \frac{\langle v^2\rangle - \langle uv\rangle}{R} \tag{16.26}$$

where $i_R(t)$ denotes the current following through the noiseless resistor R. Some of the absorbed power is re-emitted by the antenna. This corresponds to the power dissipated by the resistor R:

$$C_R = \frac{\langle (u-v)^2\rangle}{R} = \frac{\langle u^2\rangle + \langle v^2\rangle - 2\langle uv\rangle}{R} \tag{16.27}$$

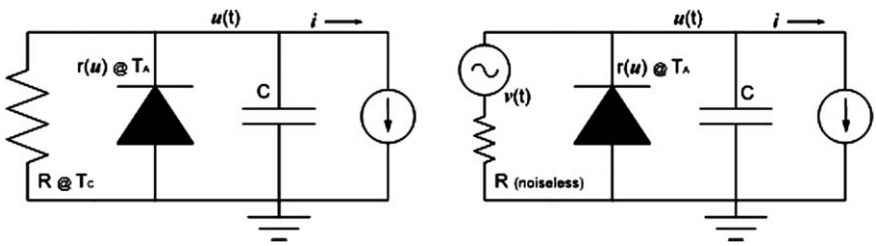

Figure 16.13 (a) Equivalent circuitry of the rectenna system: a hot resistor R at temperature T_C rectified by a diode at a lower temperature T_A; (b) the hot resistor is equivalent to a noiseless resistor and a voltage source $v(t)$ connected in series

The rest is the available power extracted from the antenna:

$$Q_R = S_R - C_R = \frac{\langle uv \rangle}{R} - \frac{\langle u^2 \rangle}{R} \tag{16.28}$$

To evaluate the first term in the expression for Q_R, the relation between u(t) and v(t) is expressed according to the Kirchoff's law:

$$v(t) = \left[1 + \frac{R}{r(u)}\right] u(t) + RC\dot{u}(t) \tag{16.29}$$

where r(u)denotes the non-linear resistance of the diode. By solving this differential equation the time average value of v(t)u(t) is found:

$$\langle uv \rangle = \lim_{T \to \infty} \frac{1}{2TRC} \int_{-T}^{T} v(t_1) e^{-\frac{t_1}{R'C}} dt_1 \int_{-\infty}^{t_1} v(t_2) e^{\frac{t_2}{R'C}} dt_2 \tag{16.30}$$

where $R' = R/[1 + \langle R/r(u) \rangle]$. The integrations can be evaluated in the frequency domain, *i.e.* expanding v(t) with v(ω) using the Fourier transformation. By considering the orthogonality of exp(iωt) components, Equation (16.30) is simplified to a resistance-independent form:

$$\langle uv \rangle = \frac{1}{RC} \int_0^{\infty} \frac{v^2(\omega) R' C}{1 + \omega^2 R'^2 C^2} d\omega = \frac{kT}{C} \tag{16.31}$$

where $v^2(\omega) = 2RkT/\pi$ is the Johnson–Nyquist noise at the low-frequency limit. This gives the first term in Equation (16.28). The second term $\langle u^2 \rangle / R$ can be calculated from the statistical distribution of the voltage, u. Its probability density has been calculated from a Markovian diffusion model proposed by Sokolov:[43]

$$p(u\,;\, i) = \begin{cases} A \exp\left(-\dfrac{Cu^2}{2kT_C}\right), u > 0 \\ A \exp\left(-\dfrac{Cu^2 + 2iuRC}{2kT_A}\right), u < 0 \end{cases} \tag{16.32}$$

where i is the extracted current through the load and A is a normalisation factor. This distribution is derived for an ideal rectifier, *i.e.* zero resistance for $u > 0$ while infinite resistance for $u < 0$. The rectified voltage $\langle u \rangle$ is calculated by the same distribution function, as well as the DC output power:

$$P(i) = i\langle u \rangle = i \int_{-\infty}^{\infty} p(u\,;\, i) u du \tag{16.33}$$

The efficiency of thermal rectification writes $\eta_{rc}(i, T_C) = P(i)/Q_R(i)$. It varies with the dimensionless current $x = iR\sqrt{C/kT_C}$, as illustrated in Figure 16.14(a). The maximum efficiency increases with the temperature of the hot resistor (Figure 16.14(b)). It is considerably lower than the Carnot efficiency, but it increases faster at higher temperatures.[43] This indicates a maximum thermal rectification efficiency of 49%, corresponding to the sun's temperature at 6000 K.

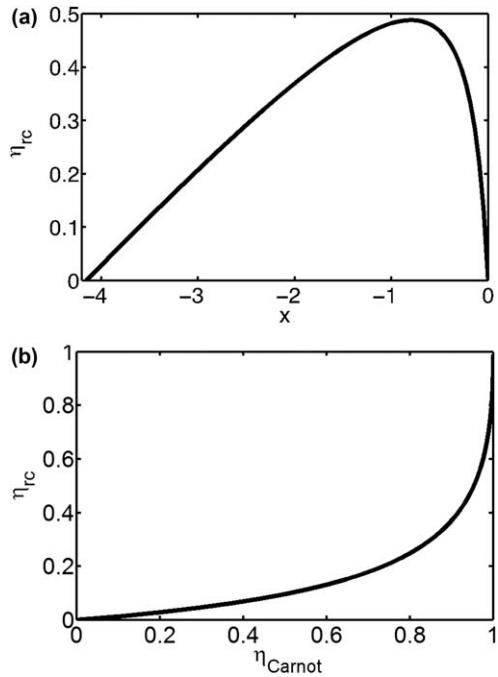

Figure 16.14 (a) The rectification efficiency η_{rc} as a function of the dimensionless current $x = iR\sqrt{C/kT_C}$. The temperature $T_C = 6000$ K ($\eta_{Carnot} = 0.95$). The maximal efficiency is attained at a finite current; (b) The maximal rectification efficiency η_{rc} as a function of η_{Carnot}. At moderate temperature differences (moderate η_{Carnot}) the efficiency of the engine is considerably lower than η_{Carnot}, but it increases rapidly when η_{Carnot} approaches unity.
Figure 16.14(b) is reproduced from Reference 43.

16.5 Quantum Rectification

In considering the rectification process one usually thinks of applying a time-varying ac voltage to a diode to produce a smoothly time-varying current. Due to the asymmetry in the diode's $I(V)$ characteristics the current flows dominantly in one direction, producing a DC current output. That is not the way that an optical rectenna works – or for that matter, any rectifier working at optical frequencies. We can gain insight into optical frequency rectification by looking at the conduction band profile of a MIM diode at different modulation frequencies. In Figure 16.15 the effect of a sub-optical-frequency AC voltage is shown. The energy difference between the left and right hand Fermi levels is modulated by the applied AC voltage.

At optical frequencies the photon energy divided by the electronic charge, $\hbar\omega/e$, is on the order of the voltage at which there is significant nonlinearity in the $I(V)$ characteristic. A semi-classical (quantum) approach is required to evaluate the tunneling current. Photon-assisted tunneling (PAT) theory was

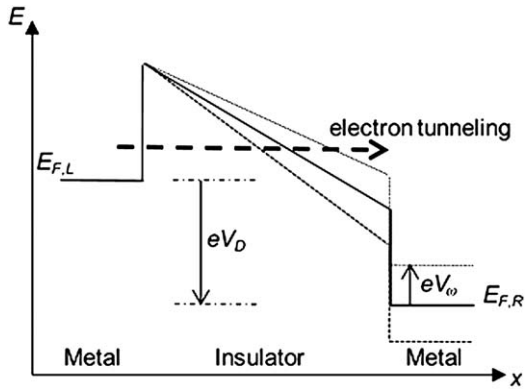

Figure 16.15 Classical model of the conduction band profile of an MIM diode modulated by a sub-optical-frequency ac voltage. The ac signal causes the Fermi level difference between the left and right sides of the tunnel junction to oscillate, which causes a change in the tunneling distance and hence in the tunnel current.
Reproduced from Grover, Joshi and Moddel.[53]

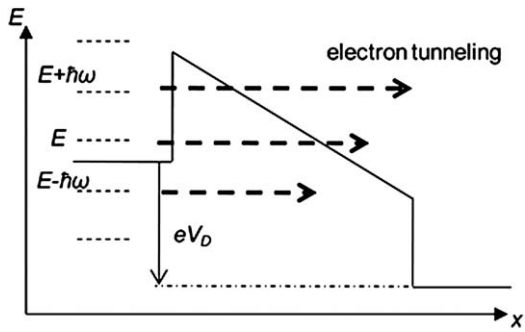

Figure 16.16 Effect of photon-assisted tunnelling (PAT) on electron tunneling through an MIM diode. The semiclassical theory gives the probabilities for electrons at energy E to absorb or emit photons and thus occupy multiple energy levels separated by $\hbar\omega$.
Reproduced from Grover, Joshi and Moddel.[53]

developed by Tien and Gordon[81] to analyze the interaction of photons in a superconducting junction and adapted to tunnel devices by Tucker and Millea.[82] The result can be seen in the effect on the conduction band profile of an MIM diode under optical frequency modulation, shown in Figure 16.16. The sea of electrons below the Fermi level in the metal conduction band now occupy multiple energy levels that are separated by $\pm\hbar\omega$ from the original energy levels, and multiples of $\hbar\omega$ for higher-order, less probable interactions.

The effect of PAT can be seen in the $I(V)$ characteristics that result. To make the illuminated $I(V)$ curve formation clear, we start with a simple piecewise linear $I(V)$ curve, shown in Figure 16.17(a). Scaled PAT components

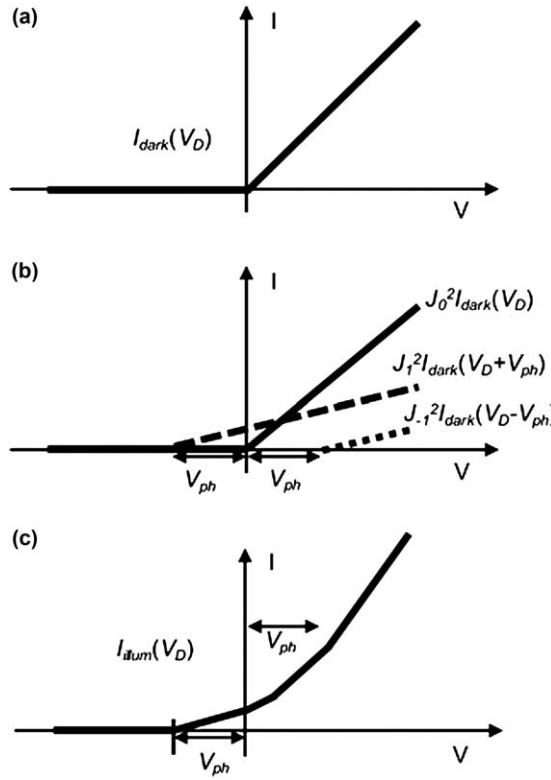

Figure 16.17 (a) Piecewise linear dark $I(V)$ curve. (b) Under high frequency illumination scaled components of the dark $I(V)$ curve shifted by $\pm \hbar\omega$ are added. (c) The illuminated $I(V)$ curve obtained by adding the components in (b).
Reproduced from Grover, Joshi and Moddel.[53]

of the dark $I(V)$ curve shifted by $\pm \hbar\omega$ are added, as shown in Figure 16.17(b), and added together to produce the resulting curve shown in Figure 16.17(c). Unlike conventional solar cells, which produce power in the 4th quadrant of the $I(V)$ curve, rectenna solar cells produce power in the 2nd quadrant.

The $I(V)$ curve in the 2nd quadrant appears to be triangular in Figure 16.17. This would give a poor maximum fill factor of 25%. In fact, when the load is matched to the diode for each voltage, corresponding to constant incident power, a more rectangular $I(V)$ curve results.[53] A more realistic set of $I(V)$ curves is shown in Figure 16.18, showing the illuminated $I(V)$ curve as more rectangular.

The quantized nature of the tunneling process affects not only the rectification process but also the diode ac resistance as seen by the antenna. At optical frequencies the rectification proceeds by discrete electron energy shifts, as opposed to the continuous variations shown in Figure 16.15. The diode ac resistance also becomes a function of the $I(V)$ curve at $\pm \hbar\omega$ about

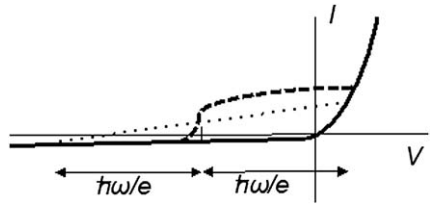

Figure 16.18 Sketch of an $I(V)$ curve for a rectenna diode. The solid curve shows the $I(V)$ for the rectenna in the dark, and the dashed curve shows the $I(V)$ under illumination. The operating voltage for the maximum power point is indicated by a small vertical line on the V axis. The secant resistance is the reciprocal of the slope of the line connecting the dark $I(V)$ curve at $\pm\hbar\omega$ about the operating voltage and is shown as a dotted line.
Reproduced from Moddel.[83]

the operating voltage. This 'secant resistance'[53] is the reciprocal of the slope of the dotted line shown in Figure 16.18. The secant resistance of the dark $I(V)$ curve determines the coupling efficiency between the antenna and diode at optical frequencies, and the conventional resistance of the illuminated $I(V)$ curve at the operating point determines the DC coupling between the diode and the load.

The quantum nature of the rectification process at optical frequencies, as described by PAT theory, has several consequences.[53] It limits the quantum efficiency of rectennas to unity, *i.e.*, one electron of current for each incident photon. It reduces the AC resistance of the diode, as compared to the small-signal differential resistance. This is good because the diode impedance must match to the low impedance of the antenna, $\sim$100 Ω, for optimal power coupling. This quantum rectification also has severe implications for the power conversion efficiency, as described in the next section.

16.6 Broadband Rectification Efficiency Limit

Microwave rectennas have demonstrated broadband power conversion efficiencies well in excess of 80%.[84] When Bailey proposed the use of optical rectennas for solar energy conversion in 1972,[18] the technology was seen as a way to break through the Shockley–Queisser limit of 34%,[85] which is function of the Trivich–Flinn limit of 44% imposed by a quantum process[86] reduced by thermodynamic considerations. Behind Bailey's proposal was the implicit assumption that rectenna rectification was not subject to the 44% limit imposed by a quantum process. Earlier in this chapter we considered the efficiency limitations based upon thermodynamic considerations. Here we explore whether Bailey's implicit assumption was correct, and what the broadband efficiency limit is based upon the actual quantum rectification process as described by photon-assisted tunneling theory.

For monochromatic illumination, the power conversion efficiency for optical rectennas can approach 100%, just as with conventional solar cells.

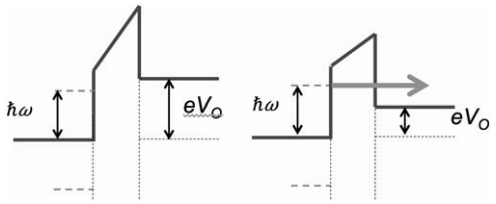

Figure 16.19 Band diagram for an MIM diode under two operating voltages, V0, under monochromatic illumination with photon energy $\hbar\omega$ (a). When $\hbar\omega < eV_0$ the electrons have insufficient energy to tunnel from the left hand metal to an empty state in the right hand metal. (b) When $\hbar\omega > eV_0$ the electrons do have sufficient energy to tunnel to an empty state.
(Unpublished, courtesy of Saumil Joshi.)

The key to achieving high efficiency is the operating voltage, V_0, assuming that other parameters such as antenna efficiency, diode $I(V)$ asymmetry, antenna-diode impedance matching are all perfect. The operating voltage is a self bias that is determined by the load resistance times the DC photocurrent. The effect of the operating voltage can be seen in the band diagrams of Figure 16.19, which are special cases of Figure 16.16. In Figure 16.19(a) the operating voltage times the electron charge (eV_0) is higher than the photon energy ($\hbar\omega$). The consequence is that the electrons excited in the left hand metal do not have sufficient energy to tunnel to an unfilled state in the right hand metal. In Figure 16.19(a) $eV_0 < \hbar\omega$ and the excited electrons can tunnel to an empty state. If $eV_0 \ll \hbar\omega$ the efficiency will be poor because only a fraction of the energy of each incident photon is used, and so the optimal efficiency results when $eV_0 \cong \hbar\omega$.

For broadband illumination from the sun optimal efficiency would result only if a different operating voltage could be selected for each photon energy region of the spectrum. Since the photocurrent from the entire spectrum is channelled to a single diode there can be only one operating voltage, and hence the power conversion efficiency is compromised. This efficiency has been calculated based on photon-assisted tunneling theory assuming perfect antenna efficiency, diode $I(V)$ asymmetry, and antenna-diode impedance matching.[54] The result is 44%, identical to the Trivich–Flinn efficiency[86] and the Shockley–Queisser 'ultimate efficiency' limit.[85] The diode operating voltage in rectenna solar cells plays the role that bandgap plays in conventional solar cells.

Bailey's original intention of exceeding the efficiency limits of a quantum process are not realized with optical rectennas. The reason that the beyond 80% power conversion efficiency of microwave rectennas does not apply here is that the microwave rectennas operate in the classical domain whereas the solar rectennas operate in the quantum regime. The classical regime applies when $\hbar\omega/e$ is much smaller than the voltage at which the $I(V)$ curve exhibits significant nonlinearity, and the photon flux is low enough that the AC voltage developed at the diode is much less than $\hbar\omega/e$.

A way to circumvent this efficiency limit would be to use some sort of a 'photon homogenizer'[83] that could process the broad band of photon energies and convert it to a single photon energy. Then a single optimal operating voltage could be used in the rectification process. In theory at least, this could be achieved by the mixing of frequencies in the diode to produce sum, difference, and harmonic frequencies. This would allow a high operating voltage corresponding to the highest photon energies of interest, and photons of lower energies would be mixed together to produce sufficient energies for the electrons to tunnel to empty states. Such mixing would require sufficiently high intensity to engage higher-order rectification processes, and it would, in fact, result in higher efficiency.[54] These higher intensities are not achievable with solar illumination for optical rectennas, even if large antennas or optical concentrators are used. The reason is that the coherence of terrestrial sunlight extends over a diameter of only 19 μm.[48] Gathering the sunlight from a larger area decreases the coherence and results in diminishing returns for the rectified current due to cancellation of out-of-phase components of the current in the diode. Without some innovation to greatly improve the nonlinearity of the diode far beyond what has been achieved for any type of room-temperature diode, or to somehow create coherence in the illumination, the ultimate conversion efficiency limit of 44% remains. As with conventional solar cells, the conversion efficiency of rectenna solar cells could be increased by splitting the spectrum and directing each spectral region to a rectenna solar cell at a different optimal operating voltage.[74] Rectennas have an inherent advantage over conventional solar cell in spectral splitting because they not require materials matched to each spectral range.

16.7 High-frequency Rectifiers

16.7.1 MIM/MIIM Rectifiers

Two types of transducers have commonly been used for IR and optical antenna devices,[4] microbolometers and metal—insulator–metal (MIM) diodes.[74] Both, but especially the microbolometer, are sensitive to the temperature of the surrounding materials. Microbolometers respond more slowly than MIM diodes, with the latter speed being limited, in theory, to about 10^{-15} s by the speed of electron tunneling through the junction. Experimental devices respond more slowly.

16.7.1.1 RC *Time Constant Limitation of MIM Diodes*

Although the transit time of electrons through the insulator is sufficiently short to allow optical frequency rectification, other constraints severely limit the response time of MIM diodes. In particular, the *RC* time constant for the antenna/diode system is the culprit.[74] In the usual rectenna circuit, the diode and the antenna are in parallel. To efficiently transfer AC power from

the antenna to the diode the resistances of the two elements must match. Since the resistance of optical antennas is on the order of 100 Ω the resistance of the diode must be similar. The *RC* time constant for the system is then the product of the parallel resistance, approximately 50 Ω, and the diode capacitance. Providing a sufficiently low resistance in the diode requires a sufficiently large area, but the larger the diode area the larger geometric capacitance will be.

For an optimal tunneling device the largest current density that can generally obtained in a tunnel current is less than 10^7 A cm^{-2}. The smallest imaginable voltage at which such a current could be produced is at least 0.5 V. Combining these two numbers gives an absolute minimum resistance of 5×10^{-8} Ω cm^{-2}. The minimum capacitance will occur for a low dielectric constant and large insulator thickness. For an insulator with a very low relative dielectric constant of 2 and a large thickness (for a tunneling device) of 5 nm, the geometric capacitance is 4×10^{-7} F cm^{-2}. Multiplying the resistance and capacitance values gives $RC = 20$ fs. The peak of the solar spectrum is at a wavelength of approximately 2 μm, which corresponds to a frequency of $f = 0.15$ PHz (0.15×10^{15} Hz). Rectifying this requires a response time of $1/2\pi f = 1$ fs, which is a factor of 20 smaller than the lowest possible *RC* time constant. The *RC* time constant for practical diodes will be even greater than 20 fs,[74] so that it is not feasible to rectify visible-light frequencies using rectennas with parallel-plate diodes.

16.7.2 New Concepts for High Frequency

Because of the *RC* limitations in MIM diodes discussed above, several alternative diodes for optical rectennas have been instigated, as discussed below.

16.7.2.1 Double-insulator MIIM Diodes

Forming a double-insulator MIIM diode can provide improved $I(V)$ characteristics over single-insulator MIM diodes. The application of resonant MIIM diodes for rectenna solar cells was proposed, simulated, and demonstrated at DC by Eliasson and Moddel[16,33] and demonstrated at 60 GHz[34] and infrared frequencies at Phiar Corporation. Hegyi *et al.*[87] simulated MIIM characteristics in the absence of resonance. Grover and Moddel[88] analyzed MIIM diodes in detail and compared their characteristics to single-insulator devices. Analysis of the $I(V)$ characteristics of MIM and MIIM diodes requires a simulator, as use of analytical tunneling theory gives incorrect results, particularly for low barrier diodes.[88] Alimardani *et al.*[89] demonstrated double-insulator diodes and Maraghechi *et al.*[90] demonstrated high-barrier triple-insulator diodes.

The advantages of MIIM diodes arise from one of two mechanisms,[88] as shown in Figure 16.20. For the example, the two types of diodes are identical except for thickness. When the left hand insulator, which has a larger electron affinity than the right hand insulator, is sufficiently thick a resonant quantum well forms in its conduction band. When the Fermi level of the left hand

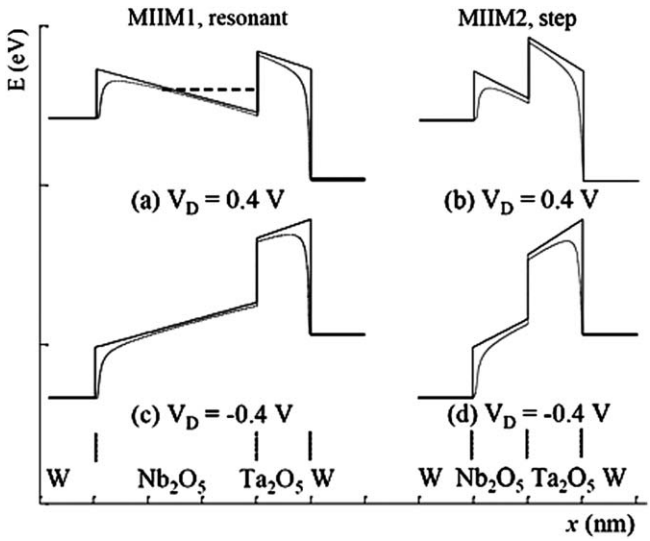

Figure 16.20 Mechanisms for enhanced nonlinearity in MIIM diodes. Energy-band profiles are shown for resonant and step MIIM diodes. Forward and reverse bias profiles are shown respectively in (a) and (c) for a resonant diode, and in (b) and (d) for a step diode. The dotted lines show the profiles with image force barrier lowering. The thickness of the Nb_2O_5 layer is the only difference between the two diodes. Reproduced from Grover and Moddel.[88]

metal rises to match the resonant level in the insulator the level provides a transport path for electrons. This produces a sharp increase in the current because the tunneling distance for electrons is reduced, and the current increases exponentially with decreasing tunneling distance. For the resonant tunneling mechanism, forward bias occurs when the Fermi level is raised for the metal adjacent to the higher electron affinity insulator. For an applied voltage of the opposite polarity, shown in Figure 16.20(c), the electrons must tunnel through all or most of the two insulators, and the current is therefore smaller than under forward bias and corresponds to reverse bias.

Alternatively, when the left hand insulator is thinner any resonant level formed would be too high to be useful. Under the polarity of bias that corresponded to forward bias for the resonant diode, shown in Figure 16.20(b), here the electrons must tunnel through both insulators. With the opposite polarity bias shown in Figure 16.20(c) electrons tunnel through only the higher-conduction-band insulator, and are then injected into the conduction band of the other insulator. For this 'step' diode the latter condition corresponds to forward bias, opposite to the resonant case. Both the resonant and the step diode mechanisms are useful. The choice depends upon the available materials and desired characteristics.

Double-insulator MIIM diodes tend to show greater nonlinearity in their $I(V)$ characteristics than single-insulator MIM diodes made using similar

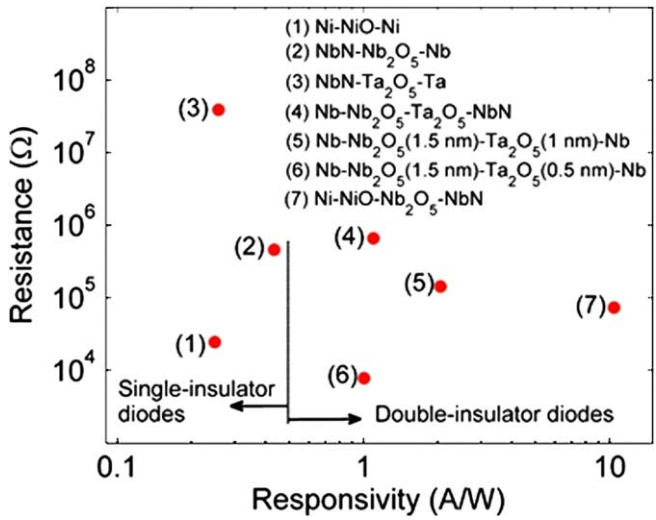

Figure 16.21 Comparison of single- and double-insulator diodes, showing resistance versus responsivity at zero bias. Rectennas require high responsivity and low resistance. The double-insulator diodes show improved performance, having smaller resistance and larger responsivity. The area for the diodes is 100×100 nm^2.
Reproduced from Grover.[52]

materials. For a rectenna two key desirable characteristics are (1) low resistance, to couple efficiently to the antenna resistance, and (2) high responsivity, which is a function of the $I(V)$ curvature as defined in Equation (16.17). In Figure 16.21 these two parameters are shown for a realistic set of materials for single and double insulator diodes. Desirable characteristics are in the lower right hand region of the plot. As can be seen from the examples shown, double-insulator diodes fall in this region and single-insulator diodes do not.

16.7.2.2 Sharp-tip Diodes

The *RC* time constant for planar MIM diodes is independent of area because the $R \propto 1/\text{area}$ and $C \propto$ area. One way to decrease the *RC* is to change the shape of the diode. Miskovsky *et al.*[49] are developing a rectenna with a sharp tip because the constant *RC* for planar MIM devices is replaced with an *RC* that scales with $(\text{area})^{1/4}$ for a spherical tip. In Figure 16.22 a schematic for a sharp tip rectenna is shown. Fabricating such a device, in which the tip is separated from the electrode by a tunneling distance of only $\sim$1 nm, is a challenge. The ingenious way that Miskovsky *et al.*[49] accomplish this is to initially form large metal/vacuum/metal structures and then add material to the tip using atomic layer deposition (ALD). As the spacing approaches 1 nm the reactants can no longer access the tip region, and so the growth stops in a self-limiting process.

A different type of sharp tip asymmetric tunneling diode was developed by Choi *et al.*[50] It makes use of a coplanar MIM diode formed by deposition,

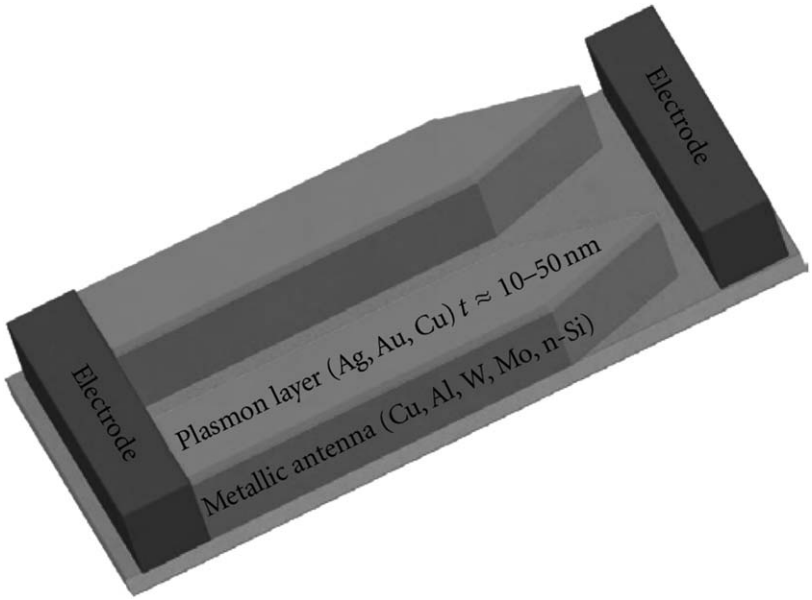

Figure 16.22 Schematic of a sharp tip rectenna. Reproduced from Miskovsky *et al.*[49]

electron-beam lithography and then strain-assisted self liftoff to form the diodes. Coupled with antennas the devices have shown asymmetric $I(V)$ characteristics and response to RF[50] and to 10.6 μm infrared radiation.[91]

16.7.2.3 Traveling-wave Diodes

Another way to avoid the diode RC time constant constraint is to using a traveling-wave configuration, so that the diode impedance is like that of a transmission line rather than a lumped element.[35,36] In such a case the characteristic impedance is largely determined by size and spacing of the structure rather than the tunneling properties. A schematic of the traveling-wave diode is shown in Figure 16.23.

Using a finite element analysis the characteristics of the traveling-wave diode were simulated.[36,92] When used as a detector with an applied bias, the traveling-wave configuration shows a responsivity for 3 μm radiation that is nearly three orders of magnitude larger than its lumped element counterpart, as shown in Figure 16.24. Further work is required to determine whether the traveling-wave diode advantages in a detector provide similar advantage for an energy harvesting device.

16.7.2.4 Geometric Diodes

The main source of capacitance in MIM diodes is between the parallel plates of the two electrodes. A totally planar device would have substantially lower

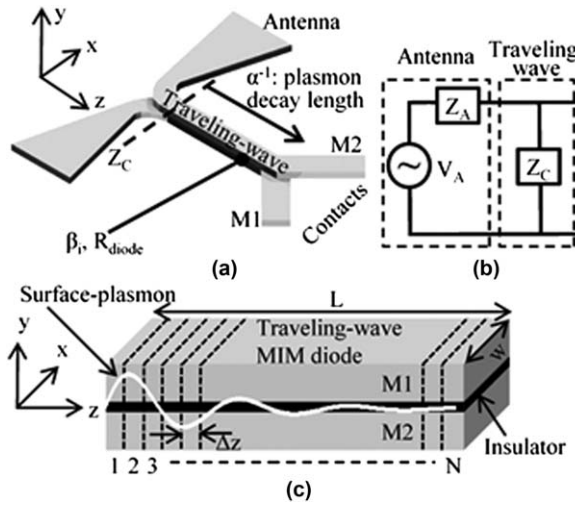

Figure 16.23 Traveling-wave diode configuration. (a) View showing the antenna arms converging into a parallel-plate waveguide with a thin insulator between the metals M1 and M2. The load is connected to the contact pads. (b) Small signal circuit model for the rectenna. The characteristic impedance of the traveling-wave diode can be readily matched to that of the antenna. (c) A 3D view of the traveling-wave MIM diode showing a surface plasmon traveling down the insulator, and decaying as it produces a rectified current.
Reproduced from Grover *et al.*[36]

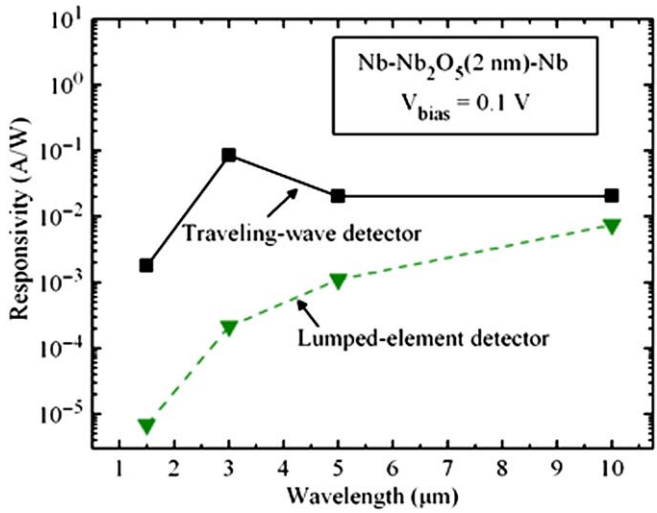

Figure 16.24 Calculated responsivity comparison of lumped-element and the traveling-wave detectors. The traveling-wave detector shows significantly better performance at smaller wavelengths.
Reproduced from Grover *et al.*[36]

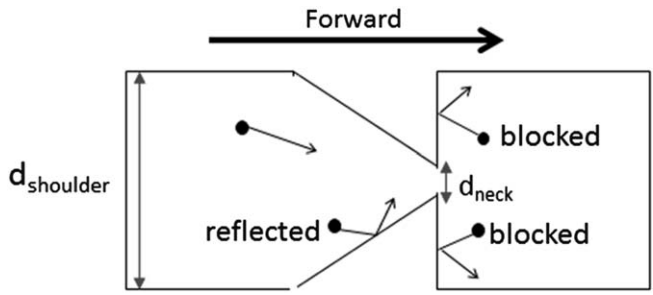

Figure 16.25 (a) Geometric diode structure. The neck width (d_{neck}) must be on the order of the carrier mean-free path length for charge carriers in the material. The charge carriers reflect at the boundaries of the device. Reproduced from Zhu *et al.*[37]

capacitance, and hence a potentially smaller *RC* time constant. The geometric diode configuration shown in Figure 16.25 is such a planar diode, and is formed from a thin conductor. On the left-hand side of the neck, the carriers moving to the right can either directly channel through the neck or reflect off the tapering edges and keep moving forward. On the right-hand side of the neck, the vertical edge blocks most of the carriers moving to the left. Hence the diode forward direction for carriers is left-to-right. The planar capacitance of such is device is calculated to be a few attofarads.[37]

To sense the device geometry the mean-free path length of the charge carriers must be on the order of the neck width of the diode. Because graphene has a particularly long mean-free path length, approaching 1 μm, it serves as an excellent material for such a diode. Optical response of graphene geometric diodes has been demonstrated for 10.6 μm radiation (corresponding to 28 THz).[37] Thus far the $I(V)$ characteristics of such devices has have been insufficiently nonlinear to provide efficient rectification, and will need to be improved if the technology is to become practical.

16.8 Summary and Conclusions

Quantum rectennas for solar application accept sunlight by using optical antennas, followed by rectification process for DC power output. This concept was proposed in 1970s and has been investigated via analogs in the fields of radio astronomy, microwave transmission and biological optical detectors. Relevant fundamental problems have been discussed in this chapter. An example of this is the partial coherence of sunlight, which limits size of the antenna or array of antennas. Quantitative analysis has demonstrated a reduced coherence efficiency at a larger field point separation. 90% coherence efficiency can only be achieved at a separation of 19 μm or less. Several approaches to antenna design, such as conical spiral antennas, have been proposed to accept both polarizations plus a bandwidth much broader than that of conventional microwave antennas. In terms of practical issues, design and fabrication of nanoscale elements are essential, due to the

shorter plasmonic wavelength and the ultrafast rectification speed. Rectification at optical frequencies also requires quantum analysis of the transport of charge carriers. The *RC* time constant of MIM diodes is too restricted, it may still be possible for new rectifier techniques to bypass this limit. Alternatives to MIM diodes include multi-insulator metal-insulator diodes, sharp-tip diodes, traveling-wave diodes, and geometric diodes. Element matching between the antenna, rectifier and filters put further restrictions on design of the rectenna solar cell.

The fundamental efficiency limit for the rectenna solar cell is still under investigation. In this chapter two different approaches are discussed, corresponding to the respective scenarios of incoherent and coherent sources. The first approach is based on rectification of thermally agitated noise and it is valid for purely incoherent black-body radiation and broadband absorption. In this situation the incident light and the antenna together are treated as a heat source connected to a cold rectifier. That rectenna system is essentially a heat engine. The rectification efficiency increases towards the Carnot efficiency for a larger temperature contrast, reaching 49% for 6000 K. Alternatively, to avoid cancellation of current in the diode due to absorption of incoherent radiation by the antenna, the antenna size and hence the current magnitude is limited. In quantum rectification in optical rectennas, the operating (bias) voltage plays the role that bandgap plays in semiconductor solar cells. The limited current magnitude along with quantum rectification process limit the efficiency for rectifying broadband solar radiation to 44%.

Acknowledgements

The contributions of FY and RC to this Program have been supported by the Australian Government through the Australian Renewable Energy Agency (ARENA). Responsibility for the views, information or advice expressed herein is not accepted by the Australian Government.

References

1. L. Novotny and N. van Hulst, *Nat. Photonics*, 2011, **5**, 83.
2. J. J. Greffet, *Science*, 2005, **308**, 1561.
3. R. L. Olmon and M. B. Raschke, *Nanotechnology*, 2012, **23**, 444001.
4. J. Alda, R.-G. J. M. J. López-Alonso and G. Boreman, *Nanotechnology*, 2005, **16**, S230.
5. D. C. Skigin and M. Lester, *J. Nanophotonics*, 2011, **5**, 050303.
6. R. Corkish, M. A. Green, T. Puzzer and T. Humphrey, Proceedings of 3rd World Conference on Photovoltaic Energy Conversion, 2003, **3**, 2682.
7. P. Muhlschlegel, H. J. Eisler, O. J. F. Martin, B. Hecht and D. W. Pohl, *Science*, 2005, **308**, 1607.
8. M. A. Green and S. Pillai, *Nat. Photonics*, 2012, **6**, 130.
9. V. P. Zhdanov and B. Kasemo, *Appl. Phys. Lett.*, 2004, **84**, 1748.
10. H. Tan, R. Santbergen, A. H. Smets and M. Zeman, *Nano Lett.*, 2012, **12**, 4070.

11. H. A. Atwater and A. Polman, *Nat. Mater.*, 2010, **9**, 205.
12. B. F. Burke and F. Graham-Smith, *An Introduction to Radio Astronomy*, Cambridge University Press, Cambridge, 1997.
13. R. Corkish, M. A. Green and T. Puzzer, *Sol. Energy*, 2002, **73**, 395.
14. D. Y. Goswami, S. Vijayaraghavan, S. Lu and G. Tamm, *Sol. Energy*, 2004, **76**, 33.
15. T. M. Razykov, C. S. Ferekides, D. Morel, E. Stefanakos, H. S. Ullal and H. M. Upadhyaya, *Sol. Energy*, 2011, **85**, 1580.
16. B. J. Eliasson, *Metal-insulator-metal diodes for solar energy conversion*, PhD Thesis, University of Colorado, 2001.
17. *Rectenna Solar Cells*, ed. G. Moddel and S. Grover, Springer, New York, 2013.
18. R. L. Bailey, *J. Eng. Power*, 1972, **April**, 73.
19. R. L. Bailey, P. S. Callahan and M. Zahn, Electromagnetic wave energy conversion research, Report NASA-CR-145876 (N76-13591), University of Florida, 1975.
20. USA Pat., 3,760,257, 1973.
21. USA Pat., 4,445,050, 1984.
22. USA Pat., 4,574,161, 1986.
23. USA Pat., 4,720,642, 1988.
24. USA Pat., 4,972,094, 1990.
25. A. M. Marks, Proceedings of the 26th Intersociety Energy Conversion Engineering Conference, ed. D. L Black, American Nuclear Society, La Grange Park, IL, 1991, 5, pp. 74.
26. Polarized Solar Electric Co., Lumeloid solutions, Available: http://www.polar-solar.com/lumeloi-solutions.html, 2009, [18 January 2013].
27. E. A. Farber, Antenna Solar Energy to Electricity Converter (ASETEC), Report AF C F08635-83-C-0136, Task 85-6, University of Florida, 1988.
28. J. D. Kraus, *Antennas*, McGraw-Hill, New York, 2nd edn., 1988.
29. J. D. Kraus and R. J. Marhefka, *Antennas for all Applications*, McGraw-Hill, Boston, 3rd edn., 2002.
30. G. H. Lin, R. Abdu and J. O. M. Bockris, *J. Appl. Phys.*, 1996, **80**, 565.
31. B. Berland, L. Simpson, G. Nuebel, T. Collins and B. Lanning, Proceedings of National Center for Photovoltaics, Program Review Meeting, 2001, pp. 323–324.
32. B. Berland, Photovoltaic Technologies Beyond the Horizon: Optical Rectenna Solar Cell, Report NREL/SR-520-33263, ITN. Energy Systems Inc., Littleton, Colorado, 2003.
33. B. J. Eliasson and G. Moddel, US Patent 6,534,784. 2003.
34. S. Rockwell, S. D. Lim, D. B. A. Bosco, J. H. Baker, B. Eliasson, K. Forsyth and M. Cromar, in Radio Frequency Integrated Circuits (RFIC) Symposium, 2007 *IEEE*, 171.
35. M. J. Estes, G. Moddel, US Patent 7,010,183, 2006.
36. S. Grover, O. Dmitriyeva, M. J. Estes and G. Moddel, *IEEE Trans. Nanotechnol.*, 2010, **99**, 716.
37. Z. Zhu, S. Joshi, S. Grover and G. Moddel, *J. Phys. D: Appl. Phys.*, 2013, **46**, 185101.

38. Y. Wang, K. Kempa, B. Kimball, J. B. Carlson, G. Benham, W. Z. Li, T. Kempa, J. Rybczynski, A. Herczynski and Z. F. Ren, *Appl. Phys. Lett.*, 2004, **85**, 2607.
39. M. Sarehraz, K. Buckle, T. Weller, E. Stefanakos, S. Bhansali, S. Krishnan and Y. Goswami, Proceedings of 31st IEEE Photovoltaic Specialists Conference, 2005, p. 78.
40. USA Pat., US2007096990-A1; US7362273-B2, 2008.
41. USA Pat., US2007069965-A1; US7486236-B2, 2009.
42. R. H. Dicke, *Rev. Sci. Instrum.*, 1946, **17**, 268.
43. I. M. Sokolov, *Europhys. Lett.*, 1998, **44**, 278.
44. D. K. Kotter, S. D. Novack, W. D. Slafer and P. Pinhero, ASME Conference Proceedings, 2008, 43208, 409.
45. R. Osgood III, S. Giardini, J. Carlson, G. E. Fernandes, J. H. Kim, J. Xu, M. Chin, B. Nichols, M. Dubey, P. Parilla, J. Berry, D. Ginley, P. Periasamy, H. Guthrey and R. O'Hayre, SPIE (*Int. Soc. Opt. Eng.*), Plasmonics: Metallic Nanostructures and Their Optical Properties IX, ed. M. I. Stockman, 2011, 8096, 809610.
46. J. M. Nunzi, ed. D. L. Andrews, J. M. Nunzi and A. Ostendorf, SPIE, Nanophotonics III, 2010, 7712, 771204.
47. R. M. Metzger, *Synth. Met.*, 2009, **159**, 2277.
48. H. Mashaal and J. M. Gordon, *Opt. Lett.*, 2011, **36**, 900.
49. N. M. Miskovsky, P. H. Cutler, A. Mayer, B. L. Weiss, B. Willis, T. E. Sullivan and P. B. Lerner, *J. Nanotechnol*, 2012, 512379.
50. K. Choi, *IEEE Trans. Electron Dev.*, 2011, **58**, 3519.
51. M. Gallo, L. Mescia, O. Losito, M. Bozzetti and F. Prudenzano, *Energy*, 2012, **39**, 27.
52. S. Grover, *Diodes for optical antennas*, PhD Thesis, University of Colorado, Boulder, 2011.
53. S Grover, S. Joshi and G. Moddel, *J. Phys. D: Appl. Phys.*, 2013, **46**, 135106.
54. S. Joshi and G. Moddel, *Appl. Phys. Lett.*, 2013, **102**, 083901.
55. F. V. Dwivedi, Proceedings of International Symposium on Microwave, Antenna, Propagation and EMC Technologies for Wireless Communications, 2005, 342.
56. G. A. E. Vandenbosch and M. Zhongkun, *Nano Energy*, 2012, **1**, 494.
57. J. C. Mankins, *Space Solar Power. The First International Assessment of Space Solar Power: Opportunities, Issues and Potential Ways Forward*, International Academy of Astronautics, 2011.
58. N. Komerath, V. Venkat and J. Fernandez, Space, Propulsion & Energy Sciences International Forum SPESIF-2009, Huntsville, Alabama, 2009, 149.
59. W. C. Brown, *IEEE Trans. Microwave Theory Technol.*, 1984, **MTT-32**, 1230.
60. R. Lomas, *The Man Who Invented the Twentieth Century*, London, 1999.
61. B. P. Motjolopane and R. van Zyl, *J. Eng., Design Technol.*, 2009, **7**, 282.
62. B. F. Burke and F. Graham-Smith, *An Introduction to Radio Astronomy*, Cambridge University Press, Cambridge, 1997.
63. M. A. Green, *Third Generation Photovoltaics: Ultra-High Efficiency at Low Cost*, Springer, New York, 2006.
64. É. Verdet, *Leçons d'optique physique*, Imerie Impériale, 1870.

65. M. Born and E. Wolf, *Principles of Optics*, Cambridge University Press, 7th edn., 1999.
66. L. Mandel and E. Wolf, *Optical Coherence and Quantum Optics*, Cambridge University Press, 1995.
67. R. Winston, Y. Sun and R. G. Littlejohn, *Opt. Commun.*, 2002, **207**, 41.
68. G. S. Agarwal and E. Wolf, *Opt. Lett.*, 2004, **29**, 459.
69. A. M. Song, *Appl. Phys. A: Mater. Sci. Process.*, 2002, **75**, 229.
70. R. H. DuHamel and J. P. Scherer, *Antenna Engineering Handbook*, ed. R. C. Johnson McGraw-Hill, New York. 3rd edn., 1993, p. 14.
71. D. S. Filipovic and T. Cencich, *Antenna Engineering Handbook*, ed. J. L. Volakis. McGraw-Hill, 4th edn. 2007.
72. V. A. Podolskiy, A. K. Sarychev and V. M. Shalaev, *J. Nonlinear Opt. Phys. Mater.*, 2002, **11**, 65.
73. O. Y. Semchuk, M. Willander and M. Karlsteen, *Semicond. Phys., Quantum Electron. Optoelectron*, 2001, **4**, 106.
74. S. Grover and G. Moddel, *IEEE J. Photovoltaics*, 2011, **1**, 78.
75. J. O. McSpadden, L. Fan and K. Chang, *IEEE Trans. Microwave Theory Technol.*, 1998, **46**, 2053.
76. T. Razban, M. Bouthinon and A. Coumes, *IEE Proc., H: Microwaves, Opt. Antennas*, 1985, **132**, 107.
77. J. J. Nahas, *IEEE Trans. Microwave Theory Technol.*, 1975, **MTT-23**, 1030.
78. Raytheon, Reception - conversion subsystem (RXCV) for microwave power transmission System, Final Report, 1975, Report ER75-4386, NASA-CR-145917, Raytheon Co., Pasadena, 1975.
79. W. C. Brown, *J. Microwave Power*, 1970, **5**, 279.
80. E. C. Jordan and K. G. Balmain, *Electromagnetic Waves and Radiating Systems*, Prentice-Hall, Englewood Cliffs, 2nd edn. 1968.
81. P. K. Tien and J. P. Gordon, *Phys. Rev. Lett.*, 1963, **129**, 647.
82. J. R. Tucker and M. F. Millea, *Appl. Phys. Lett.*, 1978, **33**, 611.
83. G. Moddel, *Rectenna Solar Cells Rectenna Solar Cells*, ed. G. Moddel and S. Grover, Springer, New York, 2013, p. 3.
84. J. A. Hagerty, T. Zhio, R. Zane and Z. Popovic, Proceedings of The Government Microcircuit Applications and Critical Technology Conference, Las Vegas, 2005, 1.
85. W. Shockley W and H. J. Queisser, *J. Appl. Phys.*, 1961, **32**, 510.
86. D. Trivich and P. A. Flinn, in *Solar Energy Research*, ed. J. A. Duffie and F. Daniels, University of Wisconsin Press, Madison, 1955.
87. B. Hegyi, A. Csurgay and W. Porod, *J. Comput. Electron.*, 2007, **6**, 159.
88. S. Grover and G. Moddel, *Solid-State Electron.*, 2012, **67**, 94.
89. N. Alimardani and J. F. Conley, *Appl. Phys. Lett.*, 2013, **102**, 143501.
90. P. Maraghechi, A. Foroughi-Abari, K. Cadien and A. Y. Elezzabi, *Appl. Phys. Lett.*, 2012, **100**, 113503.
91. F. Yesilkoy, S. Potbhare, N. Kratzmeier, A. Akturk, N. Goldsman, M. Peckerar and M. Dagenais, in *Rectenna Solar Cells*, Springer, New York, 2013, p. 163.
92. X. Lei and V. Van, *Opt. Commun.*, 2013, **294**, 344.